UNIVERSITY OF CALIFORNIA
Santa Barbara

Hydraulic Bores Propagating into Shear Flow

A thesis submitted in partial satisfaction
of the requirements for the degree of

Master of Science

in

Mechanical Engineering

by

Joshua Novins

Committee in Charge:

Professor Eckart Meiburg, Chair

Professor Frederic Gibou

Professor Paolo Luzzatto-Fegiz

September 2017

The thesis of
Joshua Novins is approved:

Professor Frederic Gibou

Professor Paolo Luzzatto-Fegiz

Professor Eckart Meiburg, Committee Chairperson

September 2017

Abstract

Hydraulic Bores Propagating into Shear Flow

Joshua Novins

Internal bores, also know as internal hydraulic jumps, can develop from phenomena in both oceanic and atmospheric situations. Classical approaches handle these bores in cases when density differences between the two layers are large, and more sophisticated approaches can now predict the bore height and propagation velocity in certain cases when the two layers have similar densities. These two-layer models, which conserve mass separately in each layer while conserving momentum across both layers, can generate reasonable predictions for bore velocity if the up and downstream layer heights are known. Traditionally, these models have needed to make assumptions about restricting the energy loss to either the upper or lower layer, but these assumptions are made unnecessary by utilizing conservation of vorticity. Within this work we propose utilizing vorticity conservation to first close the system of equations; after doing so, the energy drop across the bore can be calculated analytically. If we then enforce conservation of energy a predicted downstream layer height for bores can be generated that fits our analytical assumptions. By using this method we compare these model predictions to two-dimensional direct numer-

ical simulations and find that it is possible to predict bore velocity, geometry, and to a lesser extent downstream behavior based on initial conditions only.

Chapter 1

Analytical models for Boussinesq internal jumps

Existing models of two-layer internal bores tend to focus on the case of a bore propagating into still water. While Klemp et al. (1997) do present several cases of Boussinesq internal jumps propagating into shear, their conclusion that the classical approach to assuming energy loss is confined to the lower layer is unsatisfactory.

In order to make the problem of bore propagation more analytically tractable several assumptions have classically been made (Rayleigh, 1914): the bore propagates at a steady velocity U, the pressure field far up- and downstream of the front is hydrostatic, and viscous effects are negligible. Hydraulic bores

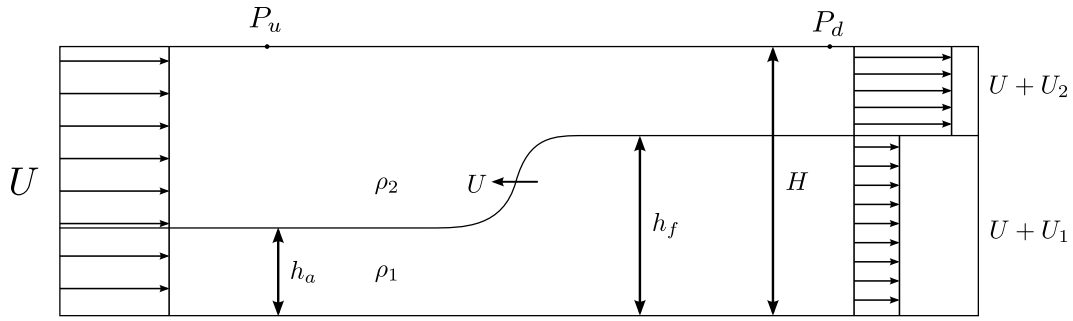

Figure 1.1: Bore propagating into still fluid in the bore reference frame. The bore itself is stationary in this frame. The x axis is oriented parallel to the channel; the y axis is oriented perpendicular to the channel. The bore is moving with some velocity U in the lab reference frame; the other velocities are in the bore reference frame (and so the bore in this reference frame is stationary).

of this state are said to be conjugate if the up and downstream layers are smooth and they can be linked via a permanent front. Looking at a control volume around the front of the jump and assuming no entrainment as seen in figure 1.1, any model must enforce the conservation of mass within each layer, along with the conservation of overall streamwise momentum

$$(U + U_1)h_f = Uh_a, \tag{1.1}$$

$$(U + U_2)(H - h_f) = U(H - h_a), \tag{1.2}$$

$$\int_0^H (P_u + \rho(y)U^2)\ dz = \int_0^H (P_d + \rho(y)U_r(y)^2)\ dz, \tag{1.3}$$

where U is the bore velocity, U_1 and U_2 are the layer velocities far downstream of the bore, $U_r(y)$ is the downstream fluid velocity as a function of y, and P_u

and P_d indicate the hydrostatic pressure plus the pressure at the top of the channel (P'_u and P'_d) at streamwise locations far up- and downstream of the front. As discussed in Borden and Meiburg (2013), Klemp et al. (1997), Wood and Simpson (1984), and any paper attempting to deal with hydraulic bore propagation, these three equations are insufficient to solve for the three unknowns U, U_1, and U_2 because (1.3) introduces another unknown: the pressure drop along the top wall of the channel, $P'_u - P'_d$. While prior work made an assumption about the location of the energy loss to achieve a solvable system of equations, Borden and Meiburg (2013) utilized conservation of vorticity rather than momentum conservation as the third equation. In the Boussinesq range, the vorticity conservation equation does not include any pressure term and thus no energy assumptions need to be made. Following the circulation-based approach therein, it should be possible to analyze the propagation of hydraulic jump into shear flow.

Chapter 2

Analytical models for Boussinesq internal jumps propagating into shear

2.1 Continuous shear

Consider a reference frame moving with a hydraulic bore with the same geometric parameters h_a, h_f, H as in figure 1.1 but allow there to be a continuous shear profile upstream of the bore, with the flow achieving a maximum velocity of $U + \frac{\Delta U}{2}$ along the bottom of the channel and a minimum velocity of $U - \frac{\Delta U}{2}$ at the top of the channel as shown in figure 2.1. We will call this case

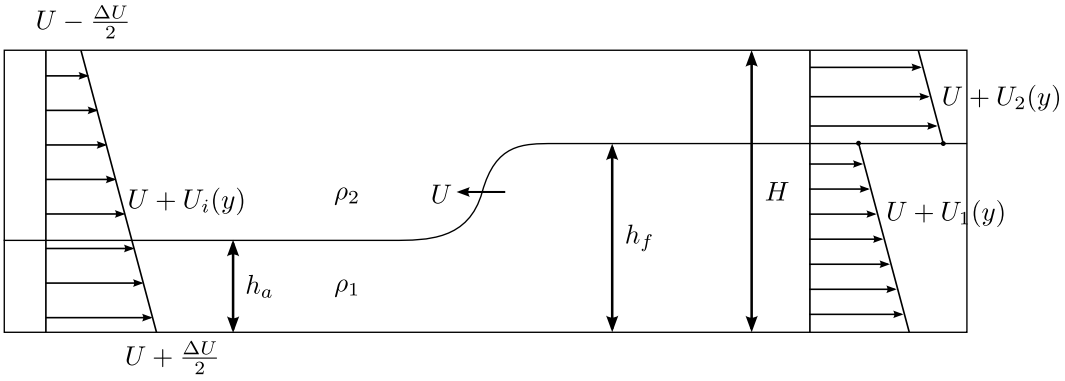

Figure 2.1: Bore propagating into a continuous shear profile in the bore reference frame. The bore itself is stationary in this frame. The x axis is oriented parallel to the channel; the y axis is oriented perpendicular to the channel. The bore is moving with some velocity U in the lab reference frame; the other velocities are in the bore reference frame (and so the bore in this reference frame is stationary).

CS for continuous shear from here on. In this CS case, the velocity profiles of the fluid upstream of the bore are

$$U_i(y) = U + \frac{\Delta U}{H}(\frac{H}{2} - y) \tag{2.1}$$

while the lower/upper layer velocity profiles downstream of the bore are

$$U_1(y) = U_1(h_f) + \frac{\Delta U}{H}(h_f - y) \tag{2.2}$$

$$U_2(y) = U_2(h_f) + \frac{\Delta U}{H}(h_f - y) \tag{2.3}$$

respectively, where y is defined as the height above the bottom of the control volume. It is important to note that the $U_1(h_f)$ and $U_2(h_f)$ are respectively

the bottom and top layer velocities after the bore at the interface in the lab reference frame.

This leaves us with 3 unknowns, the bore velocity U and the interface velocities after the bore $U_1(h_f)$ and $U_2(h_f)$. To facilitate analysis we will solve for $U + U_1(h_f)$ and $U + U_2(h_f)$ rather than $U_1(h_f)$ and $U_2(h_f)$ directly. We use mass conservation for both the upper and lower layers to generate two equations:

$$\int_0^{h_a} U + \frac{\Delta U}{H}(\frac{H}{2} - y)dy = \int_0^{h_f} U + U_1(h_f) + \frac{\Delta U}{H}(h_f - y)dy \tag{2.4}$$

$$\int_{h_a}^{H} U + \frac{\Delta U}{H}(\frac{H}{2} - y)dy = \int_{h_f}^{H} U + U_2(h_f) + \frac{\Delta U}{H}(h_f - y)dy. \tag{2.5}$$

Now, we will follow the methodology in Borden et al. (2013) by integrating the vorticity equation

$$\mathbf{u} \cdot \nabla\omega = -g'\frac{\partial \rho*}{\partial x} + \nu\nabla^2\omega \tag{2.6}$$

over the control volume to obtain a governing relation

$$\oint \omega\mathbf{u} \cdot \mathbf{n}\, dS = \iint -g'\frac{\partial \rho*}{\partial x}\, dA + \oint \frac{1}{Re}\nabla\omega \cdot \mathbf{n}\, dS. \tag{2.7}$$

where ω is the vorticity normal to the flow, ν the kinematic viscosity, and $\rho* = \frac{\rho-\rho_2}{\rho_1-\rho_2}$ is the Boussinesq density. After following the simplifications in Borden and Meiburg (2013) and neglecting viscosity we generate a vorticity relation

$$\frac{1}{2}((U + U_2(h_f))^2 - (U + U_1(h_f))^2) = g'(h_f - h_a), \tag{2.8}$$

with a Boussinesq reduced gravity $g' = g\frac{\rho_1-\rho_2}{\rho}$, and a Boussinesq reference density $\rho_0 \approx \rho_1 \approx \rho_2$. Using the nondimensional terms $R = \frac{h_f}{h_a}$ and $r = \frac{h_a}{H}$ and nondimensionalizing all velocities by $\sqrt{g'h_a}$ so that $\Delta\dot{U} = \frac{\Delta U}{\sqrt{g'h_a}}$ and nondimensionalizing all lengths by h_a, equation 2.8 becomes

$$\frac{1}{2}((\dot{U} + \dot{U}_2(R))^2 - (\dot{U} + \dot{U}_1(R))^2) = R - 1. \tag{2.9}$$

Additionally, expanding equations 2.4 and 2.5 and solving for $\dot{U} + \dot{U}_1(R)$ and $\dot{U} + \dot{U}_2(R)$ results in

$$\dot{U} + \dot{U}_1(R) = \frac{\dot{U}}{R} + \frac{\Delta\dot{U}}{2}(\frac{1}{R} - \frac{r}{R} - rR) \tag{2.10}$$

$$\dot{U} + \dot{U}_2(R) = \dot{U}\frac{1-r}{1-Rr} + \frac{\Delta\dot{U}}{2}\frac{(1 + r(-1 + r - 2R + rR^2))}{1-Rr}. \tag{2.11}$$

Again defining some intermediate variables

$$B_1 = \frac{1}{2}(\frac{1}{R} - \frac{r}{R} - rR), \tag{2.12}$$

$$B_2 = \frac{1}{R}, \tag{2.13}$$

$$B_3 = \frac{1}{2}\frac{(1 + r(-1 + r - 2R + rR^2))}{1 - Rr}, \tag{2.14}$$

$$B_4 = \frac{1 - r}{1 - Rr}, \tag{2.15}$$

and inserting 2.10 and 2.11 into 2.8, a quadratic equation is generated:

$$\dot{U}^2(B_4^2 - B_2^2) + \dot{U}(2\Delta\dot{U}(B_3B_4 - B_1B_2)) + (\Delta\dot{U}^2(B_3^2 - B_1^2) - 2(R-1)) = 0. \tag{2.16}$$

We can solve for $\dot{U}_1(R)$ and $\dot{U}_2(R)$ by inserting the solution $\dot{U}$ into 2.10 and 2.11.

Looking at figure 2.2 we can see a contour plot of the resulting bore velocities for fixed values of r. Of note is the "saddle" behavior of the velocity, as well as the regions (in the top left and bottom right on the figure) where the bore velocity is predicted to be negative.

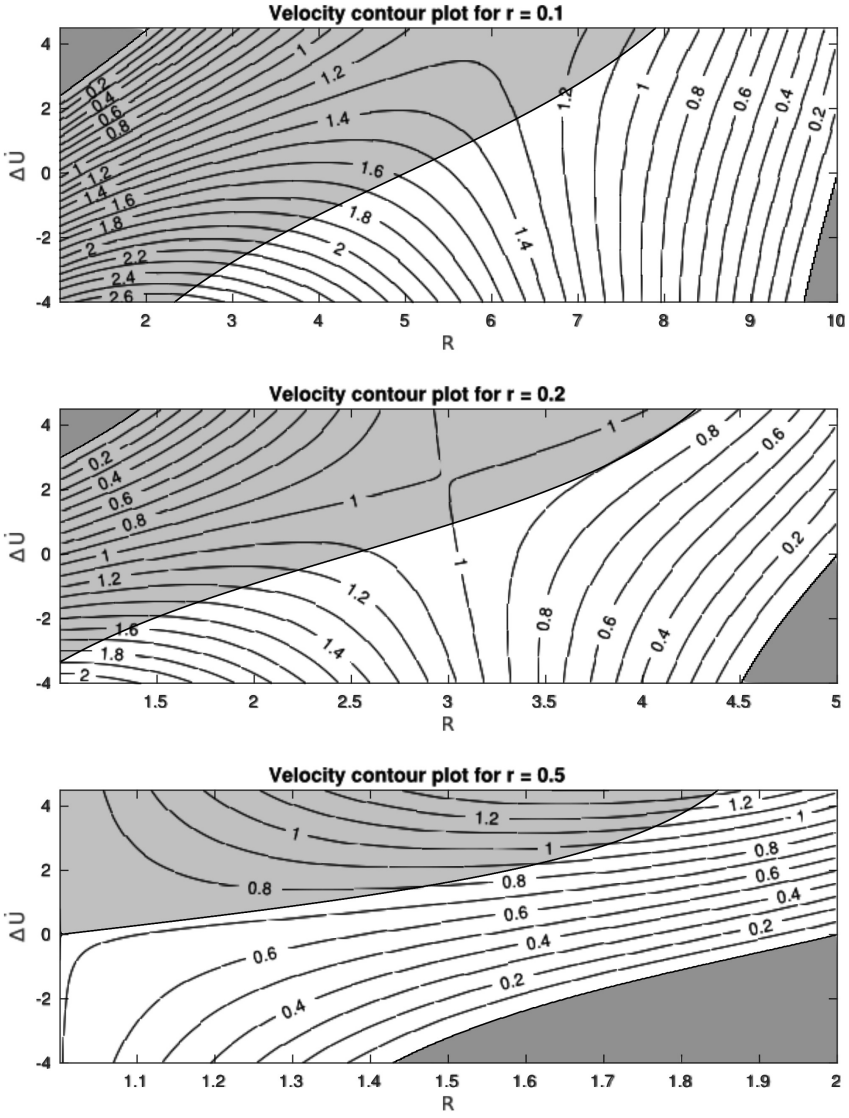

Figure 2.2: Velocity contour plots for the continuous shear case. $r = 0.1$, $r = 0.2$, $r = 0.5$ from top to bottom. $\Delta\dot{U}$ is on the y axis, R is on the x axis. The light grey shaded region has a predicted energy drop across the bore; the dark grey shaded region violates the assumption that the bore is moving with a positive velocity.

2.2 Shear jump at interface

Consider a hydraulic bore with the same geometric parameters as above in figure 1.1, but this time allow the velocity of the upper and lower layer upstream of the bore in the lab reference frame to be $-\frac{\Delta U}{2}$ and $+\frac{\Delta U}{2}$ respectively. We will call this case SJ for shear jump from here. Following the same approach as in section 2.1, the resulting equations governing the flow become:

$$(U + \frac{\Delta U}{2})h_a = (U_1 + U)h_f \tag{2.17}$$

$$(U - \frac{\Delta U}{2})(H - h_a) = (U_2 + U)(H - h_f) \tag{2.18}$$

$$U \cdot \Delta U - g'(h_f - h_a) = (U_1 - U_2)(U + \frac{U_1 + U_2}{2}) \tag{2.19}$$

where ΔU is the shear between the layers upstream of the jump. These three equations are solvable for the unknowns U, U_1, and U_2. We can once again nondimensionalize lengths by h_a to get $R = \frac{h_f}{h_a}$, $r = \frac{h_a}{H}$ and velocities by $\sqrt{g'h_a}$ giving $\dot{U} = \frac{U}{\sqrt{g'h_a}}$ and $\Delta\dot{U} = \frac{\Delta U}{\sqrt{g'h_a}}$. We can then generate a quadratic equation of the single variable $\dot{U}$

$$\dot{U}^2 A_1(1+\frac{A_3}{2}) + \dot{U}\Delta\dot{U}(\frac{A_1A_4}{2} + A_2(1+\frac{A_3}{2})) + \Delta\dot{U}^2\frac{A_2A_4}{2} + (R-1) = 0. \tag{2.20}$$

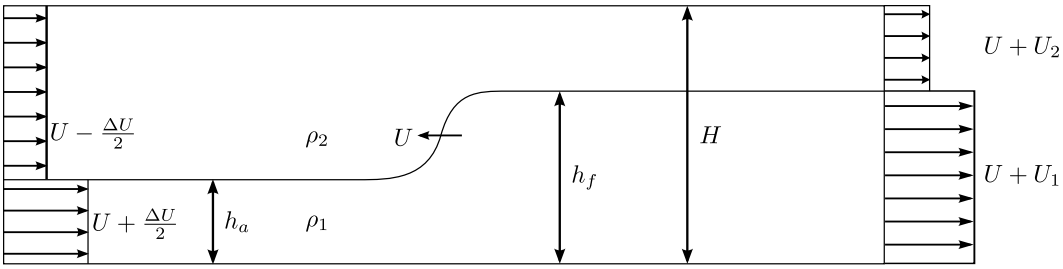

Figure 2.3: Bore propagating into a shear jump profile in the bore reference frame. The x axis is oriented parallel to the channel; the y axis is oriented perpendicular to the channel. The bore is moving with some velocity U in the lab reference frame; the other velocities are in the bore reference frame (and so the bore in this reference frame is stationary).

Several new variables are introduced, but they are functions of the geometric parameters of the problem

$$A_1 = \frac{1}{R} - \frac{1-r}{1-Rr} \tag{2.21}$$

$$A_2 = \frac{1}{2R} + \frac{1-r}{2(1-Rr)} \tag{2.22}$$

$$A_3 = \frac{1}{R} + \frac{1-r}{1-Rr} - 2 \tag{2.23}$$

$$A_4 = \frac{1}{2R} - \frac{1-r}{2(1-Rr)} \tag{2.24}$$

After solving (2.20) for $\dot{U}$, $\dot{U}_1$ and $\dot{U}_2$ can be found from

$$\dot{U}_1 = (\dot{U} + \frac{\Delta\dot{U}}{2})\frac{1}{R} - \dot{U} \tag{2.25}$$

$$\dot{U}_2 = (\dot{U} - \frac{\Delta\dot{U}}{2})\frac{1-r}{1-Rr} - \dot{U}. \tag{2.26}$$

Once again, we have generated a closed-form expression for $\dot{U}$, $\dot{U}_1$, and $\dot{U}_2$ without making any assumptions about energy.

If we look at figure 2.4 which is a velocity contour plot of the above results, we see some similarities to the CS case seen in figure 2.2. In both cases, there are regions where the predicted velocity is negative. As we will see in section 3, this does not change much in practice: regions with very high shears upstream of the bore generate large Kelvin-Helmholtz instabilities which prohibit bore development. Also, rather than saddle-type behavior we see that the behavior appears to have a "hump" where the predicted velocities are largest for middling values of R while larger/smaller values of R generate slower velocities.

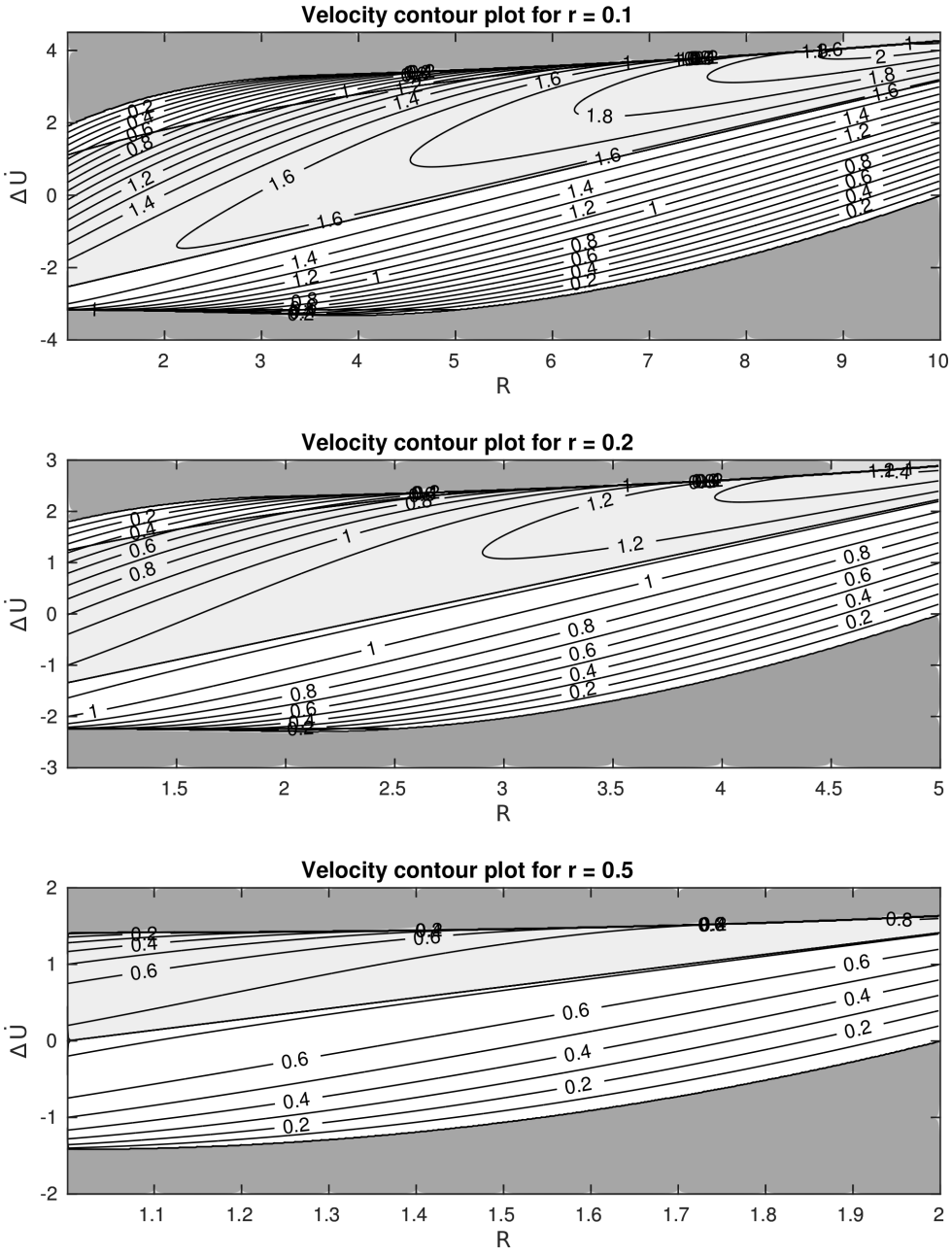

Figure 2.4: Velocity contour plots for the shear jump case. $r = 0.1$, $r = 0.2$, $r = 0.5$ from top to bottom. $\Delta\dot{U}$ is on the y axis, R is on the x axis. The light grey shaded region has a predicted energy drop across the bore; the dark grey shaded region violates the assumption that the bore is moving with a positive velocity.

Chapter 3

Comparison of model predictions to simulation results

In order to assess the validity of the predictions made by the circulation model, we will present comparisons with two-dimensional DNS results. These are obtained by our simulation code TURBINS (Nasr-Azadani and Meiburg, 2011), which employs a finite-difference discretization combined with a fractional projection method and TVD-RK3 time integration. A brief outline of the approach to the simulation will be found below; further numerical details and result validation can be found in Nasr-Azadani and Meiburg (2011) and Nasr-Azadani et al. (2013).

Fluid motion is handled with the Navier-Stokes equations with the Boussinesq approximation

$$\nabla \cdot \dot{\mathbf{U}} = 0,$$

$$\frac{\partial \dot{\mathbf{U}}}{\partial t} + \dot{\mathbf{U}} \cdot \nabla \dot{\mathbf{U}} = -\nabla \dot{P} + \frac{1}{Re} \nabla^2 \dot{\mathbf{U}} + \dot{\rho} \mathbf{e}^g,$$

where $\dot{\mathbf{U}}$ represents the fluid velocity vector, $\mathbf{e}^g$ and Re represent the gravity unit vector and the Reynolds number $Re = \frac{u_b H}{\nu}$, respectively, where u_b, H, and ν are the buoyancy velocity, total channel height, and kinematic viscosity.

The density field $\dot{\rho}(\dot{\mathbf{x}}, \dot{t})$ is described utilizing a continuum description and evolving it in an Eulerian manner by

$$\frac{\partial \dot{\rho}}{\partial \dot{t}} + \dot{\mathbf{U}} \cdot \nabla \dot{\rho} = \frac{1}{ReSc} \nabla^2 \dot{\rho}.$$

Where Sc represents the Schmidt number associated with the diffusion of the density field, $Sc = \frac{\nu}{D}$, where ν is the kinematic viscosity and D is the mass diffusivity. Generally $Sc >> 1$, although trial simulations suggest the precise value of Sc has only a weak influence on results so long as $Sc \geq O(1)$ (Hartel et al., 2000). For this reason $Sc = 6$ in all simulations.

The domain mesh uses a channel of varying sizes, with inflow and outflow boundaries in the horizontal direction. The grid is uniformly spaced with

$\Delta\dot{x} = 0.2$ and $\Delta\dot{y} = 0.0083$. The top and bottom walls use the free-slip boundary conditions for velocity and no-flux conditions for the density field, and all flow variables $\dot{q}$ are convected out of the domain at the outlet via the outflow boundary condition

$$\frac{\partial \dot{q}}{\partial \dot{t}} + \dot{\mathbf{U}} \frac{\partial \dot{q}}{\partial \dot{x}} = 0,$$

where $\dot{\mathbf{U}}$ represents the maximum fluid velocity in the domain.

The initial conditions for the simulation are generated as follows. First, the bore front is placed at some $\dot{x}'$. The initial location of the bore varies from simulation to simulation, depending on both the size of the domain and whether the bore tends to move up- or down-stream of the initial location. From there, a concentration field is generated using a sharp interface with the shape of an error function of the form

$$h_s(\dot{x}) = \frac{1}{2} \cdot (h_f - h_a) \cdot (1 + erf((\dot{x} - \dot{x}') * 2)) + h_a. \tag{3.1}$$

Where $h_s(\dot{x})$ is the height of the interface and $\dot{x}'$ is the initial location of the bore center. In this case 2 is a constant that is used to shape the error function; changing this value (within reasonable bounds) has no effect on the long-term behavior.

Next, the velocity field is generated: the velocity field is generated such that to the left (upstream) of the interface the velocity field is equivalent to the far upstream layer velocities and to the right (downstream) of the interface the velocity field is equal to the downstream layer velocity. There is a sharp transition between the two regions. The initial horizontal velocities are set to the predictions made by the circulation model; the initial vertical velocity is zero throughout the domain.

There is an initial period of transient behavior while the bore shapes itself. In cases that converge to smooth steady-state behavior, this transient behavior (and the initial conditions) does not affect the long term behavior of the bore as we will see later. Instead, cases with the same upstream conditions but different initial conditions converge to the same long-term behavior. In these cases, the initial conditions do not matter.

Upon initialization, the velocity field adjusts itself to a new bore shape. Initially, Kelvin-Helmholtz vortices form downstream of the current front, as seen in figure 3.1. In some the other figures showing the bore development in time the Kelvin-Helmholtz instabilities have already been washed downstream and/or dissipated by the first shown timestep. Depending on the Reynolds number of the flow, these Kelvin-Helmholtz waves can either be washed downstream or the flow can remain turbulent (and thus unstable) (Huerre and

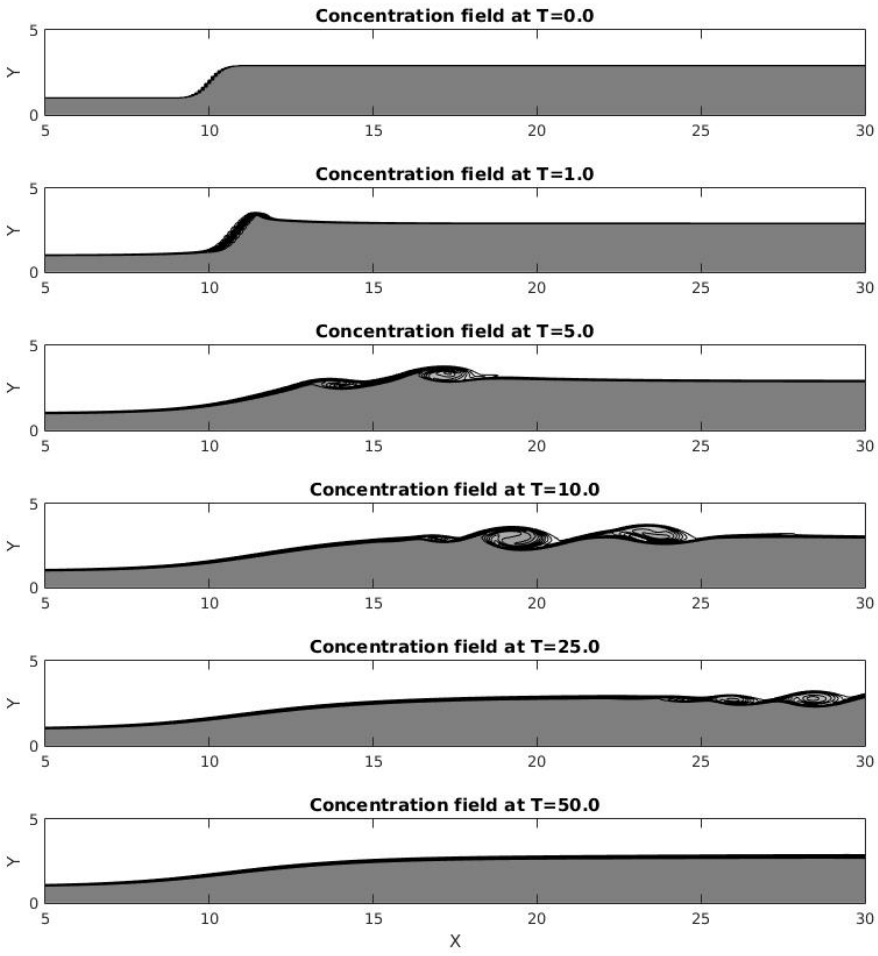

Figure 3.1: Concentration field development of a bore with parameters $r = 0.2$, $R_{initial} = 3.0$, and propagating into CS with $\Delta\dot{U} = 0.6$. Notice the initial disturbances being washed downstream, reaching a new steady layer height.

Monkewitz, 1990), with larger Re-values favoring instability. The formation of these instabilities provides an upper limit to Re in our simulation: initially, we would like a nearly-steady flowfield to compare to our model so the vortices to be washed out of the domain. This conflicts with our desire to choose Re as large as possible to minimize the effects of viscosity and diffusion, which the vorticity model does not address. These considerations resulted in us applying intermediate Re values ranging from 1500-2500 for cases that exhibit smooth behavior, depending on the specific parameters chosen. A more detailed investigation on the effects of Re number on the results can be found below in section 5.4. In some cases the shear at the interface is too large even for smaller Reynolds numbers, and so smooth nonturbulent behavior is not possible.

To facilitate analysis, our model made several notable assumptions, namely that the layer heights up and downstream of the bore were constant, had minimal mixing of the top and bottom layers, and that the bore achieves a steady state with a constant velocity. These assumptions are met among a special type of bore called conjugate state bores. To this end, the majority of the simulations analyzed in this section will be these conjugate state bores; other types of bores that do not meet our assumptions will be noted.

After running the simulations some notable parameters of the bore can be calculated. The dimensionless bore position $\dot{x_b}$ is defined to be the location in

the domain where the dimensionless depth-integrated height $\dot{h_b}$ of the lower layer is equal to $\frac{r+\frac{1}{R}}{2}$, which is the average of the up and downstream lower layer heights. Once the bore position is found, the bore velocity in the simulation reference frame is $\frac{\Delta \dot{x_b}}{\Delta \dot{t}}$ over the time frame where the bore has achieved steady behavior. We can also calculate the bore height by looking at the layer height downstream of the bore. There is some difficulty in measuring this height: in some cases, the layer height downstream of the bore is not constant. In these instances the height of the bore is defined to be the maximum layer height in the area immediately after the bore.

3.1 Continuous shear case

Returning to our analysis of the vorticity model as applied to a hydraulic jump propagating into flow with a continuous shear in section 2.1, we can generate a predicted bore velocity for any given r, initial R, and $\Delta \dot{U}$. These predicted velocities can be seen in figure 2.2. Within these tables it is important to note that the simulation bore velocity is relative to a reference frame moving with a velocity matching the vorticity model's predicted velocity. This means that the difference between this simulation reference frame velocity and the predicted velocity gives the bore's velocity relative to a stationary reference frame. To validate these predictions we ran a series of simulations for the cases

$\Delta\dot{U}$	Initial R	Final R	Simulation Bore Velocity	Initial R Model Velocity	Lab Frame Simulation Velocity	Final R Velocity	Final R Velocity Difference	Conjugate State
0.8	5.4	5	0.0749	1.4634	1.3885	1.5032	0.1147	K-H instabilities
0.8	5.8	5.01	0.0356	1.4079	1.3723	1.5024	0.1301	K-H instabilities
0.6	5.3	4.83	0.0675	1.4905	1.423	1.5362	0.1132	K-H instabilities
0.6	5.7	4.6	0.0398	1.4345	1.3947	1.5502	0.1555	K-H instabilities
0.4	5.1	4.79	0.0695	1.5309	1.4614	1.561	0.0996	K-H instabilities
0.4	5.5	4.7	0.037	1.4781	1.4411	1.5679	0.1268	K-H instabilities
0.2	4.9	4.66	0.0714	1.5722	1.5008	1.5944	0.0936	K-H instabilities
0.2	5.3	4.66	0.0373	1.5225	1.4852	1.5944	0.1092	K-H instabilities
0.0	4.8	4.55	0.0661	1.6045	1.5384	1.628	0.0896	K-H instabilities
0.0	5.2	4.5	0.0322	1.5539	1.5217	1.632	0.1103	K-H instabilities
-0.2	4.6	4.42	0.0674	1.6488	1.5814	1.665	0.0836	Small K-H downstream
-0.2	5.0	4.42	0.0353	1.6013	1.566	1.665	0.099	Small K-H downstream
-0.4	4.5	4.25	0.0631	1.6847	1.6216	1.7069	0.0853	Small K-H downstream
-0.4	4.9	4.27	0.0312	1.6362	1.605	1.7053	0.1003	Small K-H downstream
-0.6	4.3	4.17	0.0651	1.7323	1.6672	1.7435	0.0763	Small K-H downstream
-0.6	4.7	4.14	0.0348	1.6866	1.6518	1.7459	0.0941	Small K-H downstream
-0.8	4.2	4.07	0.06	1.7719	1.7119	1.7835	0.0716	Small K-H downstream
-0.8	4.6	4.01	0.0309	1.7252	1.6943	1.7883	0.094	Small K-H downstream
-1.0	4	3.93	0.0623	1.8227	1.7604	1.8286	0.0682	Small K-H downstream
-1.0	4.4	3.93	0.0339	1.779	1.7451	1.8286	0.0835	Small K-H downstream
-4.0	2.5	2.18	0.0539	2.6549	2.6167	2.6802	0.0635	No K-H instabilities
-4.0	4.0	2.18	0.0505	2.3484	2.6201	2.6802	0.0601	No K-H instabilities

Table 3.1: Simulation behavior for the CS case with $r = 0.1$. The simulation bore velocity is the velocity of the bore in a reference frame moving with the vorticity model's predicted velocity for the initial parameters (the model predicted velocity). The lab frame simulation velocity is bore's velocity to a stationary observer. The simulation bore velocity is then equal to the difference between the simulated and predicted velocity. The lab frame velocity is then compared to the predicted velocity when using the steady-state R value found in column 3, and that difference can be seen in column 8. The last two entries are the exception; the simulation velocity was set to 2.6706 to minimize the bore's movement.

$\Delta\dot{U}$	Initial R	Final R	Simulation Bore Velocity	Initial R Model Velocity	Lab Frame Simulation Velocity	Final R Velocity	Final R Velocity Difference	Conjugate State
1.0	2.9	3	0.0434	1.0185	0.9751	1.0035	0.0284	Yes
1.0	3.2	3.01	-0.0081	0.9641	0.9722	1.0018	0.0296	Yes
0.8	2.8	2.89	0.0407	1.0365	0.9958	1.0236	0.0278	Yes
0.8	3.1	2.9	-0.0079	0.9847	0.9926	1.0224	0.0298	Yes
0.6	2.7	2.78	0.0381	1.0566	1.0185	1.046	0.0275	Yes
0.6	3	2.8	-0.0078	1.0069	1.0147	1.0431	0.0284	Yes
0.4	2.6	2.67	0.0359	1.0787	1.0428	1.07	0.0272	Yes
0.4	2.9	2.69	-0.0078	1.0309	1.0387	1.0673	0.0286	Yes
0.2	2.5	2.56	0.0337	1.1031	1.0694	1.0961	0.0267	Yes
0.2	2.8	2.58	-0.0079	1.057	1.0649	1.0935	0.0286	Yes
0.0	2.4	2.45	0.0321	1.1299	1.0978	1.124	0.0262	Yes
0.0	2.7	2.47	-0.0077	1.0851	1.0928	1.1219	0.0291	Yes
-0.2	2.3	2.34	0.031	1.1591	1.1281	1.1549	0.0268	No (Undular)
-0.2	2.6	2.36	-0.0073	1.1156	1.1229	1.1526	0.0297	Yes
-0.4	2.1	2.22	0.0378	1.1983	1.1605	1.1887	0.0282	No (Undular)
-0.4	2.4	2.24	0.0071	1.1656	1.1585	1.1867	0.0282	Yes
-0.6	2	2.1	0.0373	1.2319	1.1946	1.2248	0.0302	No (Undular)
-0.6	2.3	2.15	0.008	1.2006	1.1926	1.2199	0.0273	Layer height after bore rising
-0.8	1.9	1.99	0.0377	1.2679	1.2302	1.2622	0.032	No (Undular)
-0.8	2.2	2.06	0.0096	1.238	1.2284	1.2558	0.0274	Layer height after bore rising
-1.0	1.8	1.88	0.0379	1.3062	1.2683	1.3018	0.0335	No (Undular)
-1.0	2.1	1.97	0.0126	1.278	1.2654	1.2941	0.0287	Layer height after bore rising

Table 3.2: Simulation behavior for the CS case with $r = 0.2$. The simulation bore velocity is the velocity of the bore in a reference frame moving with the vorticity model's predicted velocity for the initial parameters (the model predicted velocity). The lab frame simulation velocity is bore's velocity to a stationary observer. The simulation bore velocity is then equal to the difference between the simulated and predicted velocity. The lab frame velocity is then compared to the predicted velocity when using the steady-state R value found in column 3, and that difference can be seen in column 8.

when $r = 0.1$ and $r = 0.2$. For the case when $r = 0.1$ (the results of which can be seen in table 3.1), the large shears at the downstream interface meant that the majority of simulations did not generate a conjugate state bore. For the case when $r = 0.2$, the results can be seen in table 3.2.

Looking first at the case when $r = 0.1$, it is notable that the vast majority of simulations generate Kelvin-Helmholtz instabilities due to the high shear at the downstream interface. This violates our model assumption that the downstream layer heights should be constant and the layers should remain separate, which means that our predicted velocities for these simulations should be less accurate than cases where the simulations are smooth. This is generally what is seen. We will investigate these results further in section 6.1. To try to achieve a conjugate state result, the particular case of $\Delta\dot{U} = -4.0$, $r = 0.1$ was chosen to generate a final downstream lower layer height that was closer in height to the upstream lower layer height (and thus would not have as large of a shear jump at the downstream interface).

There are some difficulties in analyzing the accuracy of the predictions made by the vorticity model. In theory, using the steady-state parameter R should generate the most accurate velocity predictions. However, the difference in the predicted velocity between this R and the initial R is not large, and instead the difference between these two values is very small. To try to alleviate

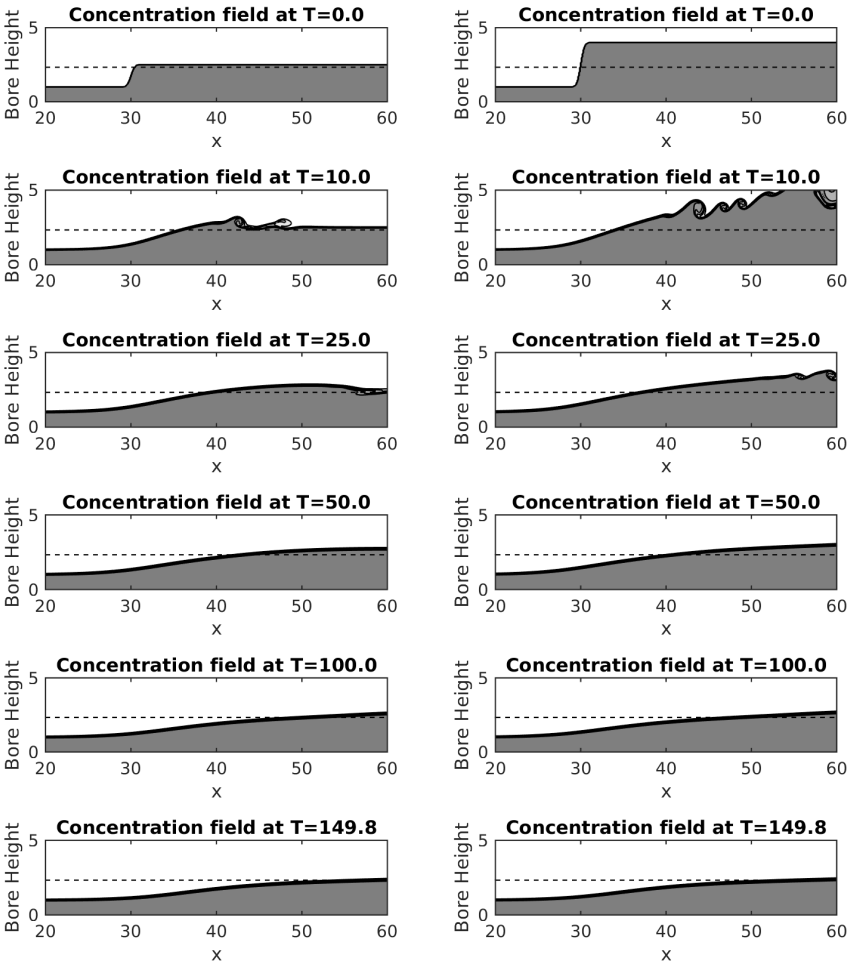

Figure 3.2: Concentration field development of a bore with parameters $r = 0.1$, $R_{initial} = 2.5$ on the left and $R_{initial} = 4.0$ on the right, propagating into CS with $\Delta\dot{U} = -4.0$. The simulation was set up with a reference frame velocity of 2.6706. The dashed line is at a height 2.33. Although not shown, the simulation domain stretches from 0 to 120 in the streamwise direction and from 0 to 10 in the spanwise direction; the shortened domain is chosen to better visualize the bore front. At the final time step the downstream layer heights were steady and achieved a constant layer height downstream of the bore.

this difficulty, we ran simulations with $R_{initial} = 4.0$ far away from the steady-state R along with a case with the same upstream conditions ($r = 0.1, \Delta\dot{U} = -4.0$) but with an initial height ($R = 2.5$) closer to the final height. These results can be seen in figure 3.2. For this simulation, the predicted bore velocity was set to be $\dot{U} = 2.6706$ for both cases (so that the bore did not move too far upstream or downstream). Just on initial visual inspection a few things are notable. Firstly, both the case starting near the steady-state R and the case further away have initial transient behavior. It's obvious that the case with the larger R has much more vigorous behavior initially, but surprisingly the development in time is very similar after this initial instabilities wash downstream. The steady-state bore behavior achieved by both cases is almost identical - both achieve a depth-integrated downstream lower layer height of 2.37 at $x = 60$ when $T = 149.8$. Using this height in the vorticity model generates the predicted steady-state velocity of $\dot{U} = 2.6674$ for both cases. Using the same methodology as earlier to track the bore velocity, the actual simulation velocities were $\dot{U} = 2.6167$ and $\dot{U} = 2.6201$ for the smaller and larger initial lower layer heights respectively. Comparing these two velocities to the velocities predicted using the initial heights $R = 2.5$ and $R = 4.0$ ($\dot{U} = 2.6549$ and $\dot{U} = 2.3484$ respectively), we see that once again there is not much improvement when using the final heights rather than the initial

heights when the two heights are close to each other. However, looking at the case with initial conditions far away from the steady state parameters the model's predicted velocity is far more accurate: the error using the final layer heights is 20% of the error as compared to using the initial layer heights in the circulation model. This shows that there could be a large improvement in accuracy for the general case with a predicted value for the downstream layer heights.

Looking next at the case when $r = 0.2$, there is a larger range of parameters where our assumptions are not violated. Intuitively, this is because the lower layer does not need to "speed up" as much to insure mass conservation when the upstream lower layer depth is thicker. When we look at the model's predicted velocity from the initial conditions against the velocities achieved by the bore in simulations with conjugate state bores, we see that the model's predicted velocity varies from the simulation velocity by 5% or less. However, we see a consistent pattern of deviations from our model: looking at the cases with the same r and $\Delta\dot{U}$ but different initial R, we see that the simulation velocities are very similar. The cases with the higher R values tend to be faster than predicted, and the cases with the lower R tend to be slower than predicted, and these velocities are extremely similar to each other.

If we look further into the simulation results we can see a reason for this: the cases with the same upstream parameters $\Delta\dot{U}$ and r converge to simulations with a similar R value. In the simulation visualized in figure 3.2, the final bore layer heights converge to nearly identical heights (less than 0.1 percent difference) despite a large difference in initial downstream layer heights; when we look at table 3.2 it can be seen that this is true for all the conjugate state cases with the same r and ΔU. When this final height is used to predict the bore velocity, we see an improvement in the precision of the model's prediction, though surprisingly there are cases where the predictions decrease in accuracy. Almost every prediction using the steady-state bore R predicts a faster velocity than what is seen in the simulation by $\tilde{0}.028$, which might point to some consistent mechanism in every case. This could be from a variety of reasons, but it is important to note that the way we defined the height of the bore (the height of the leading edge of the bore) is generally the highest point the downstream layer achieves. If smaller values for the height of R are used (which is what would happen if the height is defined further downstream) the predicted velocities would increase.

Ultimately, if there was a way to predict the height to which the bore would grow/shrink, it would be possible to improve our predictions of the bore's velocity. As we see in the cases where the bore downstream layer heights

were far from the steady-state behavior, using the final bore parameters is much more accurate than using the initial parameters. More importantly, the similarities in the steady-state behavior for cases with different initial downstream layer heights would point to there being a single steady-state conjugate state bore with the given upstream parameters.

3.2 Shear jump case

For the SJ case we see similar bore behavior to the CS case. Applying the circulation model by using the initial conditions generates velocities that are within 5% of predicted for conjugate state bores as can be seen in table 3.2. This accuracy is somewhat improved when the final height of the bore is used; the bore velocities predicted by the model using the final downstream layer height of the bore improves the predicted velocity so that the error is less than 3% in cases that are conjugate state. However, once again we see that the predicted velocities are not uniformly more accurate when the steady-state bore R is used. As discussed before, this is only the case when the initial parameters were not far from the steady-state parameters. For cases when $R_{initial}$ is far away from the steady-state R we would expect a large improvement on predicted velocity by using the steady-state R in our model.

$\Delta\dot{U}$	Initial R	Final R	Simulation Bore Velocity	Initial R Model Velocity	Lab Frame Simulation Velocity	Final R Velocity	Final R Velocity Difference	Conjugate State
1.0	3.4	3.5	-0.0183	1.1596	1.1413	1.1425	0.0012	No (K-H Instabilities)
1.0	3.8	3.53	0.052	1.0714	1.1234	1.1367	0.0133	No (K-H Instabilities)
0.8	3.2	3.27	-0.0242	1.1519	1.1277	1.1411	0.0134	Yes
0.8	3.6	3.3	0.056	1.0692	1.1252	1.136	0.0108	Yes
0.6	3	3.07	-0.026	1.1452	1.1192	1.1352	0.016	Yes
0.6	3.4	3.08	0.0484	1.0674	1.1158	1.1336	0.0178	Yes
0.4	2.8	2.86	-0.0274	1.1394	1.112	1.1315	0.0195	Yes
0.4	3.2	2.87	0.0448	1.066	1.1108	1.1301	0.0193	Yes
0.2	2.5	2.65	-0.0393	1.144	1.1047	1.1283	0.0236	Yes
0.2	2.9	2.66	0.0189	1.0868	1.1057	1.127	0.0213	Yes
0.0	2.3	2.45	-0.0413	1.1385	1.0972	1.1244	0.0272	No (Undular)
0.0	2.7	2.45	0.0133	1.0851	1.0984	1.1244	0.026	Yes
-0.2	2.1	2.22	-0.0444	1.1337	1.0893	1.1242	0.0349	No (Undular)
-0.2	2.5	2.26	0.0065	1.084	1.0905	1.1199	0.0294	Yes
-0.4	1.8	1.95	-0.0542	1.1325	1.0783	1.1266	0.0483	No (Undular)
-0.4	2.2	2.06	-0.0181	1.0996	1.0815	1.1173	0.0358	Yes
-0.6	1.6	1.69	-0.0626	1.1275	1.0649	1.1262	0.0613	No (Undular)
-0.6	2	1.93	-0.0269	1.0987	1.0718	1.1078	0.036	Yes
-0.8	1.4	1.41	-0.0771	1.1229	1.0458	1.1231	0.0773	No (Undular/ Upstream Dip)
-0.8	1.8	1.72	-0.0366	1.0983	1.0617	1.1081	0.0464	No (Undular/ Upstream Dip)
-1.0	1.2	N/A	N/A	1.1187	N/A	1.0987	N/A	No bore
-1.0	1.6	1.51	-0.0469	1.0987	1.0518	1.1089	0.0571	No (Undular/ Upstream Dip)

Table 3.3: Simulation behavior for the SJ case with $r = 0.2$. The initial R is what the simulation is initiated with; the simulation bore velocity is the velocity of the bore in a reference frame moving with the vorticity model's predicted velocity for the initial parameters (the model predicted velocity). The lab frame simulation velocity is simulated bore's velocity to a stationary observer. The simulation bore velocity is then equal to the difference between the simulated bore velocity and the circulation model's predicted velocity. The simulation's lab frame velocity is then compared to the model's predicted velocity when using the steady-state R value found in column 3, and that difference can be seen in column 8.

We continue to see that cases with the same upstream parameters tend towards the same downstream layer heights (and unsurprisingly have very similar final velocities). Unsurprisingly the vorticity model's predictions remain strongest in cases where the bore is conjugate state, as compared to cases with Kelvin-Helmholtz instabilities or undular bores.

Chapter 4

Energetics

Although we were able to predict the velocity for a bore with given geometric parameters, we have seen that the predicted behavior is dependent upon final parameters which are not necessarily close to the initial conditions. Ideally, we would like to determine a bore's velocity from an initial setup, without having to resort to referencing later geometric parameters. Using the assumptions made above, it is relatively simple to calculate the energy loss across a control volume moving with the bore velocity for a given geometry and bore velocity. It might be possible to use this energy analysis to determine what parameters a steady-state bore would tend towards.

For the CS case (looking at the top (E_U) and bottom (E_L) layer energy losses separately) we generate

$$\begin{aligned}\Delta E_{L_{CS}} &= \int_0^{h_a} (P'_u + \rho_1 gy + \frac{1}{2}\rho_1 (U + \frac{\Delta U}{H}(\frac{H}{2} - y))^2)(U + \frac{\Delta U}{H}(\frac{H}{2} - y))dy \\ &- \int_0^{h_f} (P'_d + \rho_1 gy + \frac{1}{2}\rho_1 (U_{1d}(h_f) + \frac{\Delta U}{H}(h_f - y))^2)(U_{1d}(h_f) \\ &+ \frac{\Delta U}{H}(h_f - y))dy \end{aligned} \tag{4.1}$$

$$\begin{aligned}\Delta E_{U_{CS}} &= \int_{h_a}^{H} (P'_u + \rho_2 gy + \frac{1}{2}\rho_2 (U + \frac{\Delta U}{2} - \frac{\Delta U}{H}y)^2)(U + \frac{\Delta U}{2} - \frac{\Delta U}{H}y)dy \\ &- \int_{h_f}^{H} (P'_d + \rho_2 gy + \frac{1}{2}\rho_2 (U_{2d}(h_f) + \frac{\Delta U}{H}(h_f - y))^2)(U_{2d}(h_f) \\ &+ \frac{\Delta U}{H}(h_f - y))dy \end{aligned} \tag{4.2}$$

where P'_u is the upstream top-wall pressure and P'_d is the downstream top-wall pressure. After simplifying the expressions using the continuity relation and the Boussinesq approximation as well as some algebra, it is apparent that we need to consider the top wall pressure drop; using x-momentum conservation across the same control volume generates an expression for the top-wall

pressure drop.

$$\int_0^H (P_u(y) + \rho_u(y)U_u(y)^2)dy = \int_0^H (P_d(y) + \rho_d(y)U_d(y)^2)dy \tag{4.3}$$

where $P_u(y)$, $\rho_u(y)$, $U_u(y)$ are the upstream pressure, density, and velocity profiles respectively and $P_d(y)$, $\rho_d(y)$, and $U_d(y)$ are the downstream pressure, density, and velocity profiles. After some algebra, an expression for $\frac{P'_d - P'_u}{\rho}$ can be found:

$$\begin{aligned}
\frac{P'_d - P'_u}{\rho} &= \frac{1}{4H^2(H-h_f)h_f}(h_a - h_f) * \\
&\quad (\Delta U^2(H - h_a - h_f)(-h_a^2 - h_f^2 + H(h_a + h_f)) \\
&\quad +4U\Delta U H(H - h_a)h_a \\
&\quad +2U^2 H(g' h_f(-H + h_f)(h_a + h_f) + 2H(h_a - h_f)))
\end{aligned} \tag{4.4}$$

Returning to the expression for the layer energy loss across our control volume and nondimensionalizing energy by $\dot{E} = \frac{E}{\rho g'^{\frac{3}{2}} h_a^{\frac{5}{2}}}$ we are left with

$$
\begin{aligned}
\Delta\dot{E}_{L_{CS}} &= -\frac{-1+R}{16R^2(-1+rR)}(\Delta\dot{U}(-1+r)-2\dot{U})* \\
&(\quad 4R^2(-1+rR)(-2+r+rR) \\
&\quad +\Delta\dot{U}^2(-1+r+rR)(1+R+r(-1+R(-3-2R+r(3+R^2)))) \\
&\quad -4u\Delta\dot{U}(-1+r)(-1+R(-1+r(3+R))) \\
&\quad -4u^2(1+(1+r(-3+R))R) \quad) \qquad (4.5)
\end{aligned}
$$

$$
\begin{aligned}
\Delta\dot{E}_{U_{CS}} &= \frac{(r-1)(R-1)}{16R(Rr-1)^2}(\Delta\dot{U}r-2\dot{U})* \\
&(\quad 4R(1+R)(Rr-1)^2 \\
&\quad +\Delta\dot{U}^2(-1+r+rR)(2-r(1+R)(2+R)+r^2R(3+R^2)) \\
&\quad -4\dot{U}\Delta\dot{U}(2+R(-2+R(-4+r(3+R)))) \\
&\quad -4\dot{U}^2(2+r(-3+R)R) \quad). \qquad (4.6)
\end{aligned}
$$

Both of these expressions converge at the limiting case of $\Delta\dot{U} = 0$ to the expressions found in Li and Cummins (1998).

Developing the same expressions for the SJ case, we are left with

$$\begin{aligned}\frac{P'_d - P'_u}{\rho} &= (U - \frac{\Delta U}{2})^2(1 - \frac{h_a}{H})(\frac{h_a - h_f}{H - h_f}) \\ &+ (U + \Delta U')^2 \frac{h_a}{H}(\frac{h_f - h_a}{h_f}) + \frac{g'}{2H}(h_a^2 - h_f^2), \end{aligned} \tag{4.7}$$

$$\begin{aligned}\Delta \dot{E}_{L_{SJ}} &= (1 - R)(\dot{U} + \frac{\Delta \dot{U}}{2})(\frac{1}{2}(\dot{U}^2 + \Delta \dot{U}^2)(\frac{3Rr - 1 - R - R^2 r}{(1 - Rr)R^2}) \\ &+ (\dot{U}\frac{\Delta \dot{U}}{2})(\frac{3Rr - 1 - R - 4R^2 r^2 + 3R^2 r}{(1 - Rr)R^2}) \\ &+ \frac{1}{2}(2 - r - Rr)), \end{aligned} \tag{4.8}$$

$$\begin{aligned}\Delta \dot{E}_{U_{SJ}} &= \frac{1}{2}(1 - r)(1 - R)(\dot{U} - \frac{\Delta \dot{U}}{2})((\dot{U}^2 + (\frac{\Delta \dot{U}}{2})^2)(-\frac{-3Rr + R^2 r + 2}{R(1 - 2Rr + R^2 r^2)}) \\ &- (\dot{U}\Delta \dot{U})(\frac{5Rr^2 + R^2 r^2 - 4R^2 r^3 - 2r}{Rr(1 - 2Rr + R^2 r^2)}) - 1 - R). \end{aligned} \tag{4.9}$$

By adding these expressions together ($\Delta \dot{E}_{CS} = \Delta \dot{E}_{L_{CS}} + \Delta \dot{E}_{U_{CS}}$ or $\Delta \dot{E}_{SJ} = \Delta \dot{E}_{L_{SJ}} + \Delta \dot{E}_{U_{SJ}}$) the total energy drop across the control volume is found for the CS or SJ cases.

Now that we have predictions for energy loss for a given bore velocity, it is possible to determine the energy-preserving set of parameters for a bore with given upstream flow conditions.

Chapter 5

Comparison of energy analysis to DNS results

Up to this point, we have been making the assumption that the bore is propagating between flat layers of fluid both up and downstream of the bore, which is often called conjugate state behavior. This assumption that the layers are flat will not always hold; we will discuss such cases in section 6.

Working within this assumption, we will now employ the above theoretical energy analysis in order to investigate first an interesting result from the case of a bore propagating without shear, and then progress to the SJ and CS cases. Later, we will compare these theoretical predictions against DNS simulations, paying close attention to the influence of the inflow conditions on the velocity

and energy loss of the bore using the same dimensionless quantities defined as above.

Importantly, our energy analysis looks only at the effect from the change in fluid velocity and layer height over the bore and ignores other methods of energy dissipation. Later, we will look into the effect of incorporating other energy losses; this will be more important in the cases where our assumption of conjugate state behavior does not hold.

5.1 No-shear case

Before continuing the analysis into the CS and SJ cases, it is interesting to look at the implications of applying the circulation model to a hydraulic bore propagating into still flow. Using the analysis developed by Li and Cummins (1998) for a hydraulic bore propagating with a constant, arbitrary velocity, an energy drop of

$$\dot{E}_{noshear} = \frac{1}{2}(-1+R)^2\dot{U}(1-\frac{(1+r(-2+R)R)\dot{U}^2}{R^2(-1+rR)^2}) \tag{5.1}$$

is found for some arbitrary $\dot{U}$. Taking the bore velocity predicted by the circulation model

$$\dot{U}_{noshear} = (\frac{2R^2(Rr-1)^2}{R-2Rr+1})^{1/2} \tag{5.2}$$

and inserting that bore velocity (equation 5.2) into the arbitrary $\dot{U}$ in equation 5.1 we can generate a closed-form expression for the energy loss for a bore propagating into shear-free conditions:

$$\dot{E}_{noshear} = \frac{(-1+R)^2}{\sqrt{2}}\sqrt{\frac{R^2(-1+Rr)^2}{1+R-2Rr}}(1-\frac{2(1+r(-2+R)R)}{1+R-2Rr} \tag{5.3}$$

These results are plotted in figure 5.1. It is notable that when there is no shear upstream of the bore cases with $R = \frac{1}{2r}$ (corresponding to equal layer heights after the bore) conserve energy across a control volume encompassing the hydraulic bore (again, when other forms of energy dissipation/transfer are ignored). Looking at the remainder of figure 5.1, the $R = \frac{1}{2r}$ (equivalently $\frac{h_f}{H} > \frac{1}{2}$) line splits the diagram into two sections: one with $\frac{h_f}{H} > \frac{1}{2}$ that predicts an energy increase across the bore and another with $\frac{h_f}{H} > \frac{1}{2}$ that has a predicted energy drop across the bore. We can thus see that for values of R greater than $\frac{1}{2r}$, the model predicts that there is a net energy gain across the bore: values of R larger than $\frac{1}{2r}$ are predicted to require an external energy

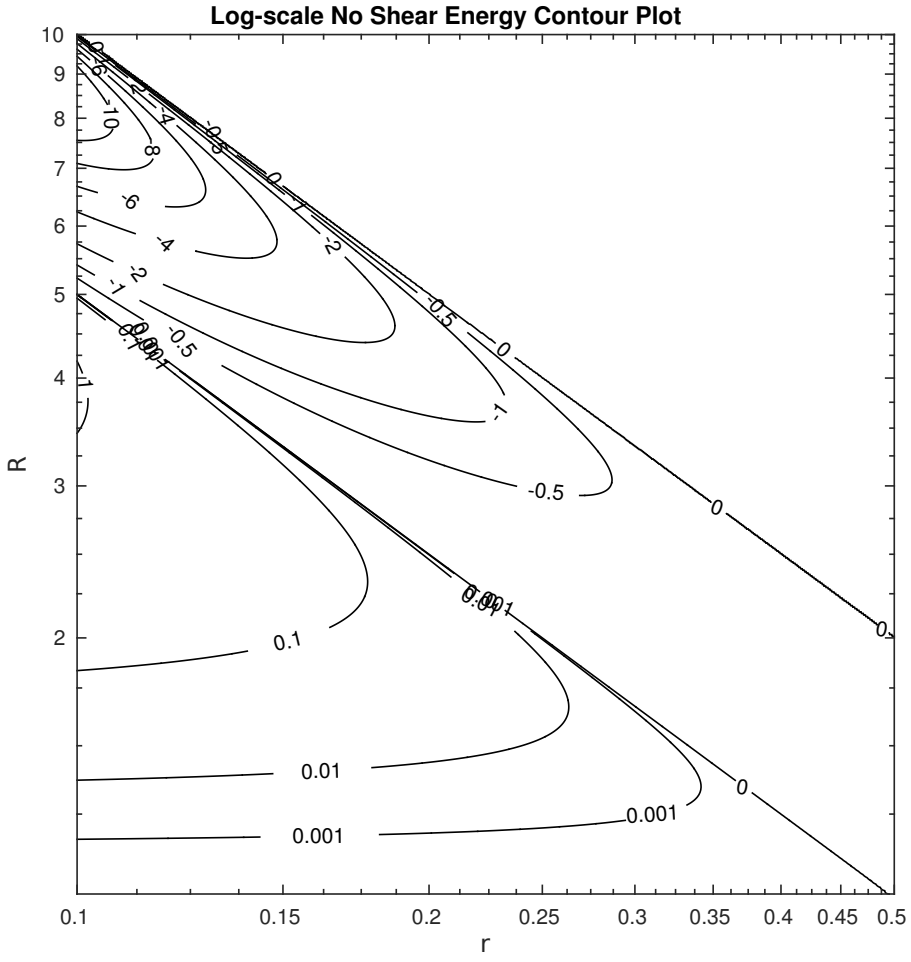

Figure 5.1: Energy contour plot on a log-log scale for the no-shear case. The topmost 0-contour line corresponds to the lower layer growing to the full channel height after the bore. The lower 0-contour line corresponds to the layer heights being equal after the bore ($R = \frac{1}{2r}$ or equivalentally $\frac{h_f}{H} = \frac{1}{2}$). Note that this is a plot of energy loss, so positive values correspond to a drop in energy across the bore.

input and are nonphysical. Alternatively, only values of R less than or equal to $\frac{1}{2r}$ are predicted to be energetically allowable.

Prior work has shown that smooth, steady bores such as we're analyzing tend be stable when the layer heights are equal after the bore (Stastna and Lamb, 2002). This result could also point to a relationship between gravity currents and hydraulic bores: similar behavior is also seen in gravity currents where a gravity current propagating into fluid without shear is stable (and has no change in energy) when the gravity current is half the channel height (Nasr-Azadani and Meiburg, 2015).

The question naturally arises as to what will happen in cases with an initial setup that is predicted to have an energy drop across the bore (or an energy gain across the bore). Within a control volume exhibiting steady behavior energy needs to be balanced between the input, output, and any possible sources or sinks. This would mean that we would expect either some form of energy dissipation and/or the bore will not be stable and it will adapt itself if there is a predicted energy drop across the bore (corresponding to cases where $R \leq \frac{1}{2r}$). As we are (for now) ignoring other forms of energy dissipation, the only other way a bore could achieve steady behavior would be for it to adapt its geometric parameters. Specifically, because the inflow shear and upstream layer heights are fixed, we would expect the bore to adjust itself to a case where

the energy input is equal to the energy output plus any dissipation. This would mean that in the absence of energy sinks such as viscous dissipation we would expect the bore to adapt to the energy-preserving case where the layer heights after the jump are equal.

To verify this hypothesis a set of simulations were run with $\Delta\dot{U} = 0$, $r = 0.2$, and $R = 2.25, 2.5$, and 3; the development of the bore is seen in figure 5.2. The simulations are set in a reference frame moving with the velocity predicted by the circulation model when $R = 2.5$. This is the height that we would expect the bore to grow/shrink towards, and so using the velocity predicted using $R = 2.5$ should generate a simulation with less upstream/downstream movement of the bore. The inflow conditions are $r = 0.2$ and $\Delta\dot{U} = 0$ (with the inflow velocities being the predicted bore velocity). Looking at the early behavior, we see that the bores behave somewhat similarly - there are instabilities generated that are then washed downstream. After these instabilities are convected out of the domain, we can see that the steady-state behavior becomes nearly identical and the downstream layer heights adapt themselves so that they are equal heights. This corresponds to the energy-preserving case in our predictions. Because the bores behave differently initially, if we look at figure 5.3 we can see that the bores shift different amounts relative to our control volume. Once that initial behavior is over we see that the bore velocities relative to the reference

frame are nearly identical: the largest difference in velocities (between the $R = 2.35$ and $R = 3.0$ cases) is less than 0.2%. These velocities in turn differ by less than 2.0% from the model's predicted velocity for the case when $R = 2.5$.

For these simulations the R values were chosen so that the bore remains conjugate state; later in section 6.2 we will investigate the case when $R = 2.0$, which is not a set of parameters that generates a conjugate state bore. From the simulation results we see that the bore grows (or shrinks) to the zero-energy case ($R = 2.5$) from the initial conditions of the simulation. This matches the what we would expect if the bore achieves an energy balance from our earlier analysis and the results from prior papers that we discussed earlier. The steady conjugate-state behavior of a bore propagating into a flow without shear is for the layer heights after the bore to achieve equal heights and for the bore to move with the velocity predicted by the circulation model for a bore with the given r and $R = \frac{1}{2r}$.

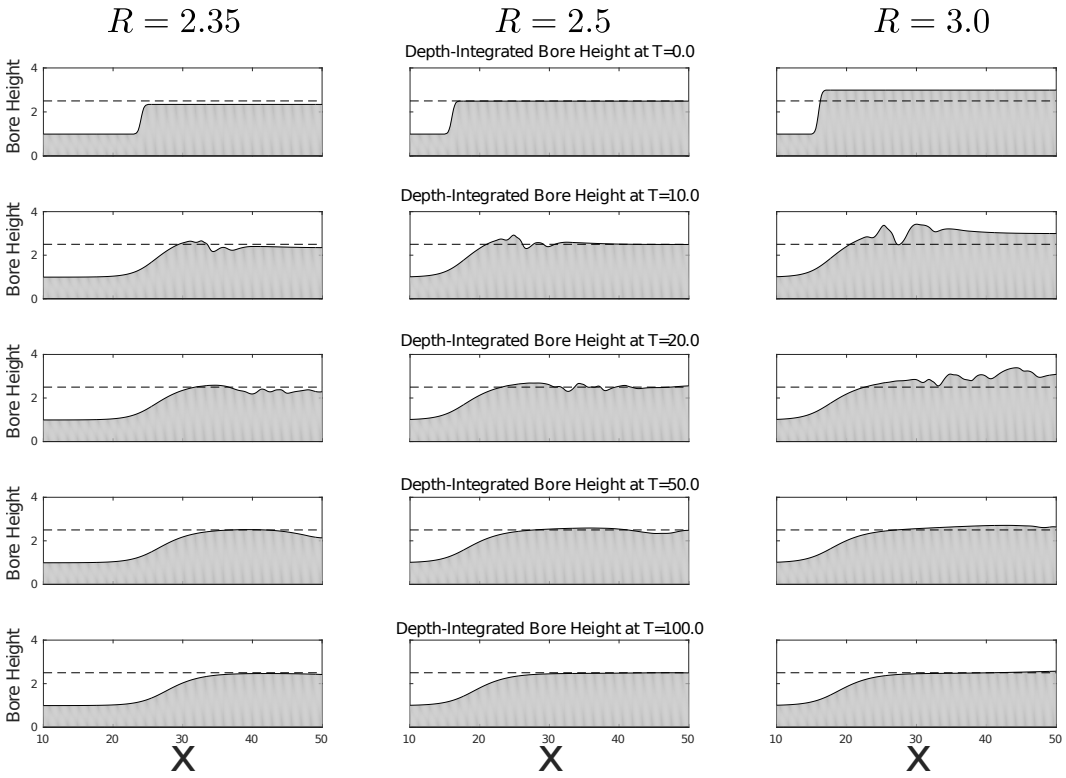

Figure 5.2: Development of three bores propagating into a flow without shear. The inflow condition is identical for all three cases: $r = 0.2$, $\Delta\dot{U} = 0$. The initial height after the jump is $R = 2.35, 2.5, 3$ respectively from left to right. The dotted line is at the half-channel height $R = 2.5$. The shaded region is the depth-integrated height. Note that for the $R = 2.35$ case the starting location is downstream of the $R = 2.5$ and $R = 3.0$ cases.

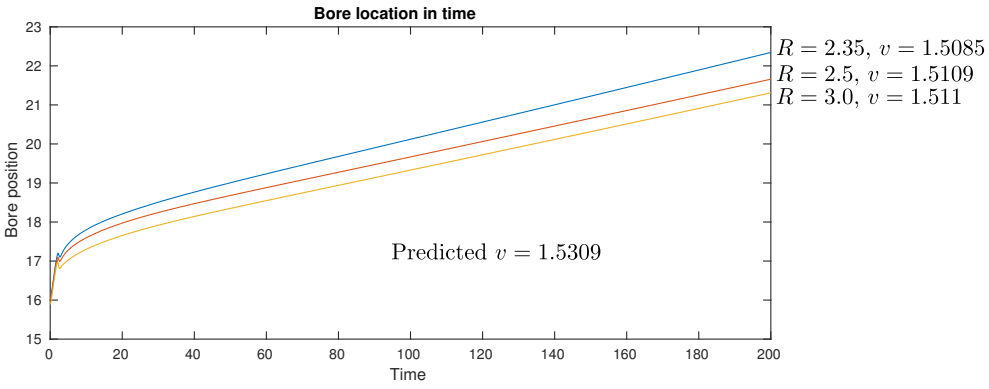

Figure 5.3: Positions in time of three bores propagating into a flow without shear. The inflow condition is identical for all three cases: $r = 0.2$, $\Delta\dot{U} = 0$. The initial height after the jump is $R = 2.35, 2.5$, or 3 (next to their respective labels on the plot). The case of $R = 2.35$ is translated by 8 to aid comparison.

5.2 Shear jump case

If we keep the layer velocities constant but allow for a shear jump at the upstream interface, we can see some interesting impacts. Looking initially at the features of the energy plot in the SJ case in figure 5.4, we see that the region where bores are physically allowable is bounded. Initially this limitation comes from our model's predicted velocity: returning back to the velocity contour plot in figure 2.4, beyond a certain positive and negative shear the predicted bore velocity is negative (the bore is travelling to the right). This violates our assumption that the bore is moving to the left. Furthermore, these regions do not generate conjugate-state behavior: simulations started in these regions have large Kelvin-Helmholtz instabilities both up and downstream of the bore

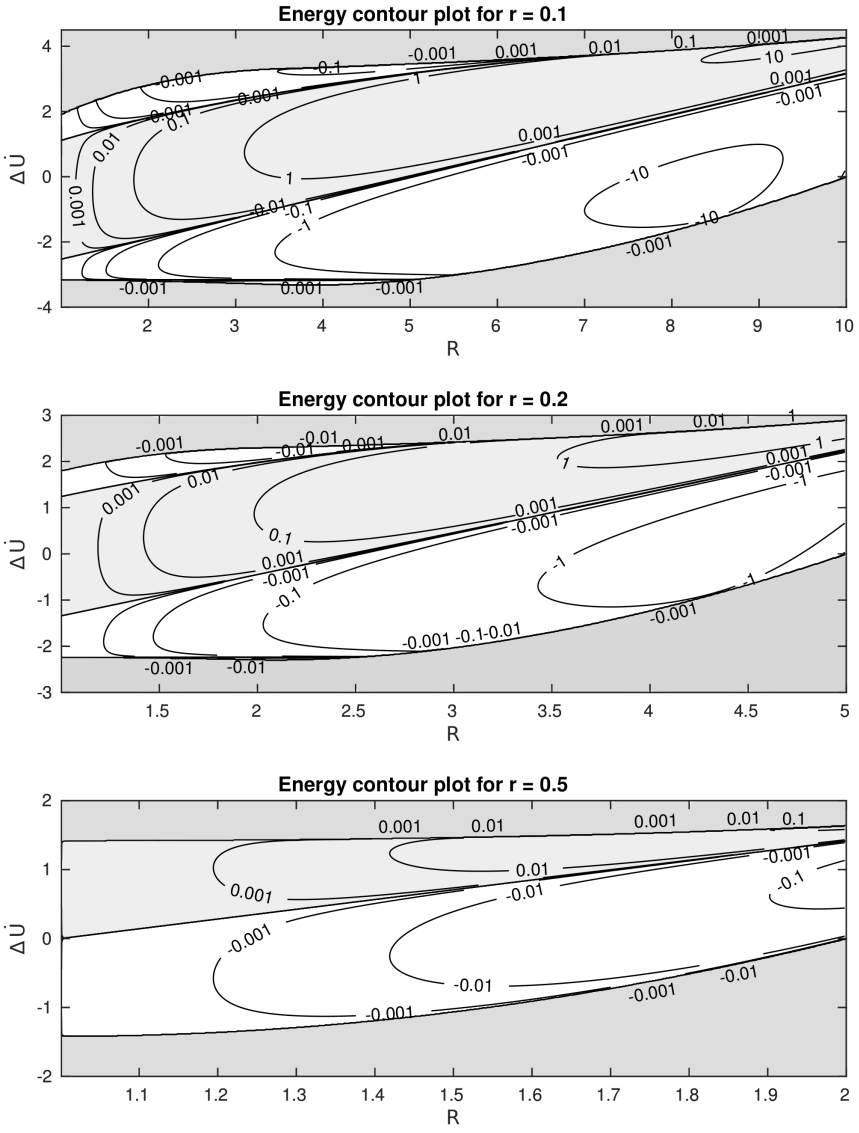

Figure 5.4: Energy contour plots for the shear jump case. $r = 0.1$, $r = 0.2$, $r = 0.5$ from top to bottom. $\Delta\dot{U}$ is on the y axis, R is on the x axis. The light grey shaded region has a predicted energy drop across the bore; the dark grey shaded region violates the assumption that the bore is moving with a positive velocity.

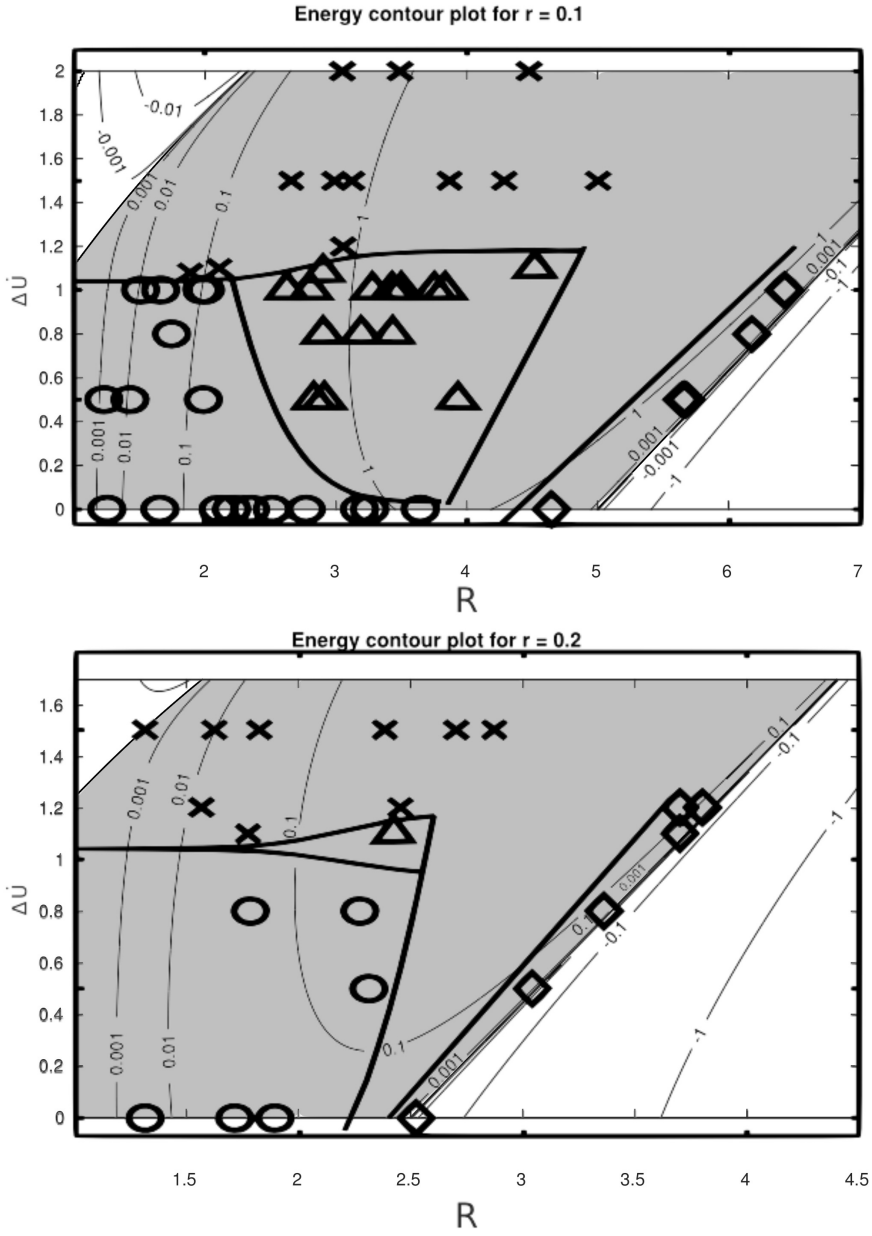

Figure 5.5: Energy contour plots for the shear jump case. $r = 0.1$, $r = 0.2$ from top to bottom. $\Delta\dot{U}$ is on the y axis, R is on the x axis. The light grey shaded region has a predicted energy drop across the bore. Each point represents the result of a numerical simulation from Ogden and Helfrich (2016). $\times$ = fully turbulent jump, $\circ$ = undular bore, $\triangle$= smooth front turbulent jump, and $\diamond$ = conjugate state.

even at low Reynolds numbers because of the high shear magnitudes. It is important to note though that these instabilities occur even at significantly lower magnitudes of $\Delta\dot{U}$ than the velocity-limiting value and simulations started in conditions with large enough $|\Delta\dot{U}|$ do not generate conjugate state bores.

Similarly to the case without shear, we can further limit the physically allowable region for SJ bores. For any given value of $\Delta\dot{U}$ bores with a predicted energy drop exist only for cases with R below some limiting value. When $\Delta\dot{U} = 0$, this value is $\frac{1}{2r}$ for all values of r as discussed earlier. As shear increases, we can see that this limiting R also increases; similarly, as shear decreases, we see that this limiting R value decreases.

First looking at the case when $r = 0.5$ in figure 5.4, we can see that no bores are energetically favorable when $\Delta\dot{U} \leq 0$. This makes intuitive sense: R must be larger than 1 by the way we defined the bore, so when $r = 0.5$ the lower layer must be greater than half the channel height after the jump (and thus has a predicted energy gain across the bore). Allowing for upstream shear changes this though: when the upstream shear $\Delta\dot{U} > 0$, it no longer remains the case that there are no bores predicted that are energy-preserving: there should be conjugate state bores with $\frac{h_f}{H}$ larger than $\frac{1}{2}$ that are energetically favorable. Just as we saw in the case without shear, if we alter the initial value of R such that the predicted energy change across the bore is nonzero,

the bore adapts itself to the energy-preserving set of parameters and moves with the velocity predicted for that set of parameters.

More changes on the energy contour plot when we shift our attention to the smaller values of r (0.1 and 0.2) as seen in figures 5.4. The general behavior remains the same - there is some maximum value of R beyond which bores of a given r and $\Delta\dot{U}$ are energetically unfavorable. However we see that rather than all cases below that particular value of R having a predicted energy drop across the bore, there are regions (with large $\Delta\dot{U}$ and small R) with a downstream layer height less than the energetically limiting value that have a predicted energy jump across the bore. These regions are not as interesting as they appear: the large shear in these regions mean that Kelvin-Helmholtz instabilities prevent bores from forming, and so we must ignore these cases in our analysis.

Returning to conditions which generate conjugate state bores, we can compare our energy analysis to prior work (Ogden and Helfrich, 2016). It's important to note that their work used the simulation final downstream layer heights, so the results seen are of bores that have achieved an energy balance. Within that paper, several regimes of bores are outlined. Thus far within this paper we have focused on conjugate state bores that are steady and have a fixed height up and downstream of the jump. In figure 5.5, we can see that in

their simulations conjugate state behavior bores tend to settle with a downstream lower layer height very close to the energy preserving values of R that our analysis found for both the $r = 0.1$ and $r = 0.2$ cases. However, cases further away from the zero-energy line do not behave as conjugate-state bores. This makes intuitive sense - cases with a large energy drop would need some other way to dissipate energy, which can result in more complicated behavior and doesn't meet all of our assumptions. Interestingly, the conjugate state bores that develop in their simulations move to a set of parameters that would generate a small predicted energy drop across the bore as compared to our energy analysis. However, our analysis does not incorporate other forms of energy dissipation. If we assume there is some dissipation in energy across the bore that we are ignoring from viscous dissipation, then the actual energy change will be lower than that found through our analysis. This unaccounted-for energy change will tend to shift the zero-energy line towards smaller values of R than our naive predictions. If we return to figure 5.5, we can see that in the Ogden and Helfrich (2016) simulations the conjugate state bores settled with values of R slightly smaller than the predicted zero-energy loss R from our analysis. This is what we would expect if viscous dissipation increases the energy drop across the control volume.

To corroborate these results, we ran a series of simulations where $r = 0.2$. As opposed to the simulations in Ogden and Helfrich (2016), we know both the initial and final set of bore parameters, the results of which can be seen in figure 5.6 and table 3.2. In general, we see similar results in the two sets of simulations - conjugate state bores achieve stable behavior with values of R slightly below the zero energy line.

Going into more detail, we can turn our attention to figure 5.6 which shows the initial and final states of the bores in our simulation. Immediately notable is that the conjugate state bores continue to achieve a steady state with values of R corresponding to very small energy drops. As mentioned earlier, this fits our hypothesis. Likewise, cases that do not achieve steady state bores tend to be further away from the zero energy line, which corresponds to a larger energy drop. These sorts of bores have more ways to dissipate energy, which means that they should need to be further into the energy drop region. There are a handful of anomalous results though for the cases with negative shears. These cases appear to achieve a steady state in regions corresponding to a small energy gain across the bore. However, these bores also do not tend to have perfectly flat downstream layer heights. It is possible that over time these bores will shrink to be in the energy region; alternatively, it is possible that

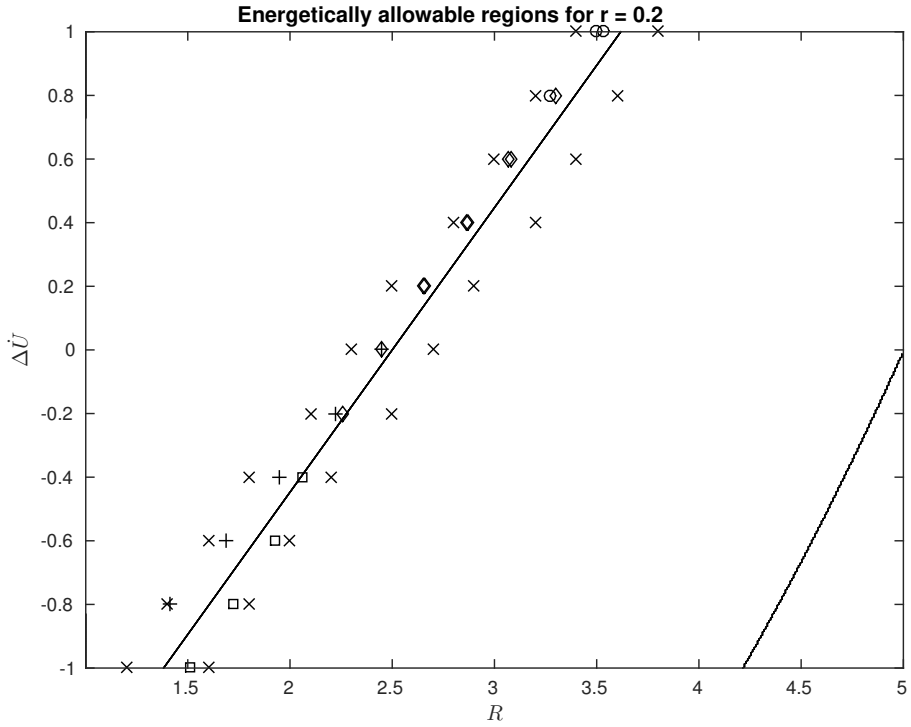

Figure 5.6: Simulations starting/ending downstream layer height ratio $R = 0.2$ along with the SJ upstream layer shear $\Delta\dot{U}$. The initial heights are labelled with an x; the steady state heights are labelled with circles, diamonds, +, and squares. Cases with circles develop downstream Kelvin-Helmholtz instabilities; cases with + develop undular waves propagating at a slower velocity than the leading wave; cases with diamonds develop into conjugate state bores; cases with squares form smooth bores that do not have a constant downstream layer height. For all cases bores with a larger initial R and the same $\Delta\dot{U}$ have a larger (or equal) final R (then the case with the same initial $\Delta\dot{U}$).

the height of the bore is being miscalculated because the downstream layer heights are growing.

It appears that we can generally predict whether a bore will be a conjugate state case or not based on how large the predicted energy change is. For cases with R slightly smaller than the zero-energy line R (at relatively low Reynolds numbers) the bore will tend toward conjugate state behavior. Furthermore, for cases further away (with smaller R values) undular bores will tend to develop in the absence of Kelvin-Helmholtz instabilities. Likewise, cases with an R that has a predicted energy jump across the bore will tend toward the zero energy R. The layers downstream of the bore will adjust themselves to a configuration that preserves energy.

Earlier, we mentioned that it seemed that bores with identical upstream parameters tended towards an identical steady-state downstream lower layer height ratio R. So far, it seems that the value for R can generally be predicted by using our energy analysis; by using this coupled with the circulation model it appears that we can generally predict bore geometry and velocity with minimal knowledge of the downstream conditions.

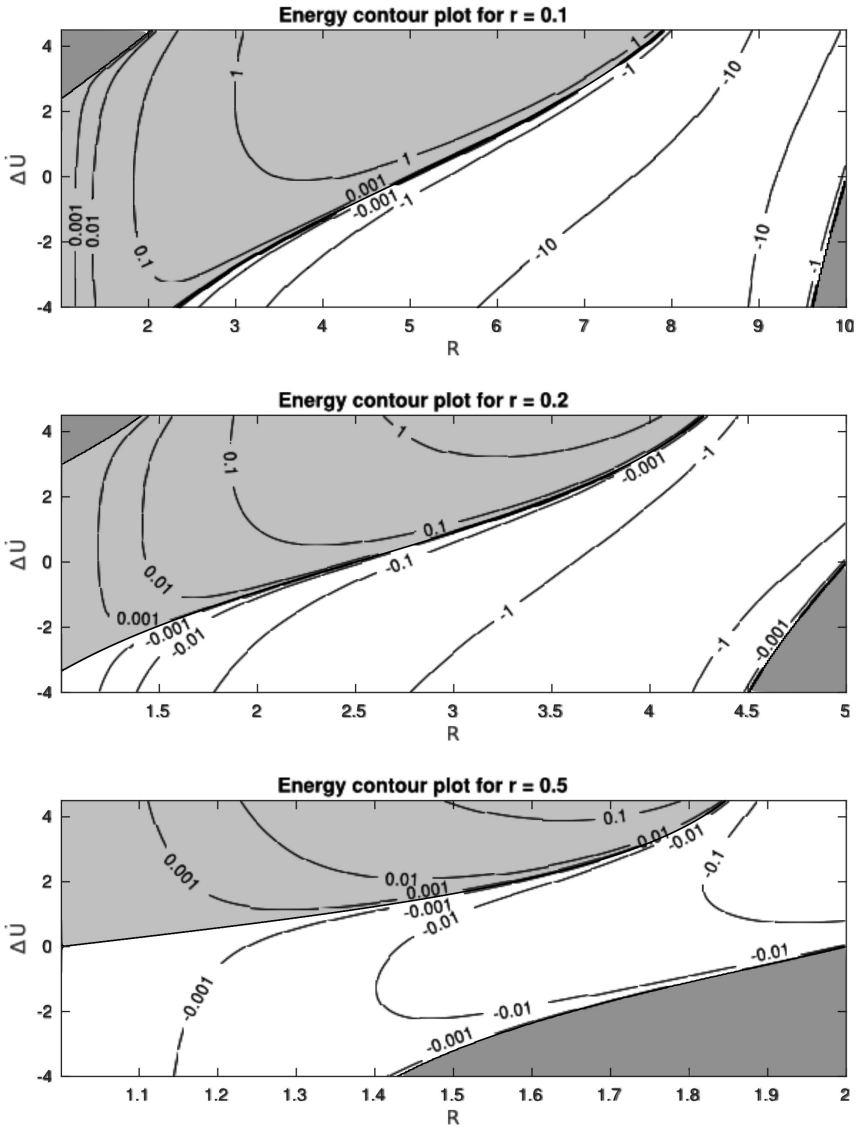

Figure 5.7: Energy contour plots for the continuous shear case. $r = 0.1$, $r = 0.2$, $r = 0.5$ from top to bottom. $\Delta\dot{U}$ is on the y axis, R is on the x axis. The light grey shaded region has a predicted energy drop across the bore; the dark grey shaded region violates the assumption that the bore is moving with a positive velocity.

5.3 Continuous-shear case

For the CS case the energetically possible cases remain strongly dependent on shear. Looking at figure 5.7, there is again some maximum R beyond which the energy analysis predicts an energy gain across the bore for a given upstream layer height r and shear $\Delta\dot{U}$. Similarly to the SJ case, this maximum height varies strongly with $\Delta\dot{U}$: as $\Delta\dot{U}$ increases or decreases, so too does the maximum R.

Many of the conclusions drawn from the SJ analysis can be applied to the CS case. First recalling the analysis for the case without shear in section 5.1, we found that lower layer heights greater than half the channel height after the shear are energetically unfavorable. This can be seen in figure 5.7; for all three lower layer heights upstream of the bore, downstream lower layer heights larger that $R = \frac{1}{2r}$ fall in the region with a predicted energy jump (if shear is zero). While (as expected) $\Delta\dot{E} = 0$ when $R = \frac{1}{2r}$, for cases where the shear is nonzero that no longer remains the case. Increasing the shear makes higher values of R energetically feasible: for cases with positive shear, it is possible to have a bore with a downstream lower layer height greater than half the channel height.

This can be seen within figure 5.7: for the case when $r = 0.5$ there are no cases that do not require energy input along the $\Delta\dot{U} = 0$ line (when $R = 1$

there is no bore). However, like the SJ analysis, in cases with a positive shear there are bores that are predicted to be energetically feasible with R larger than $\frac{1}{2r}$. Looking back at figure 5.7 to see what happens when $r = 0.1$ or $r = 0.2$, we see generally similar behavior to the SJ case (and the $r = 0.5$ case). As $\Delta\dot{U}$ increases, the predicted energy-preserving case corresponds to a larger R; as $\Delta\dot{U}$ decreases, the opposite occurs.

Similarly to the SJ case there are regions (dark grey in figure 5.7) where our assumption that the bore is moving right to left is violated. This occurs for all three cases when R is large alongside strong negative $\Delta\dot{U} = 0$; in the cases where $r = 0.1, 0.2$ this occurs when there is a very large positive $\Delta\dot{U}$ and small values of R as well. This will be discussed further below in section 6, but neither of these cases results in a steady bore: the large positive shear upstream of the bore results in Kelvin-Helmholtz instabilities that do not achieve statistically steady behavior. Unlike the SJ case though there is no natural upper/lower limit on the shear beyond which the bore velocity violates our assumption. However, this does not change the analysis for the conjugate state behavior - at sufficient shear Kelvin-Helmholtz instabilities are generated which mean that the layer heights are not constant with a sharp interface.

A series of simulations were run for the cases when $r = 0.1$ and $r = 0.2$, the results of which can be seen in figure 5.9 and in figure 3.1 from section 3.1

as well as in table 5.3. In these we can see that the bore shifts the downstream lower layer heights before it achieves steady state behavior, similarly to the no-shear and SJ cases. This steady group of parameters is again very close to the predicted zero-energy case that was calculated in section 4 and moves with the velocity the circulation model predicts for these parameters. This would seem to verify our earlier analysis. Additionally, one interesting case will be presented where the downstream lower layer height is greater than half the channel height, a situation that earlier we showed is only possible for bores with upstream shear.

If we look first at figure 5.9, we initially see that the general behavior of different initial downstream conditions achieves very similar steady-state geometries. For the case when $r = 0.1$, we see that all of the cases chosen generate large enough shears at the downstream interface so that Kelvin-Helmholtz instabilities form. In these cases, the bores achieve a steady state in the physically predicted region. However, the steady state geometries have a smaller R than would be predicted if we ignored all sources of dissipation. This makes sense; the Kelvin-Helmholtz instabilities should introduce exactly the sort of dissipation that we ignored in our earlier analysis.

All of the cases plotted in figure 5.9 exhibit Kelvin-Helmholtz instabilities downstream of the bore. Earlier, a case was investigated with upstream

geometry $r = 0.1$ and $\Delta\dot{U} = -4.0$ (figure 3.1). In this instance, two different initial downstream geometries resulted in the same steady state geometry ($R = 2.33$) and exhibited conjugate state behavior. In this instance, $R = 2.33$ corresponded exactly to the case where there is no expected energy loss in our naive analysis. As mentioned earlier, this case also illustrates the independence of the steady-state geometries from the initial downstream conditions for conjugate state bores.

Moving our attention to the case where $r = 0.2$, the steady-state behavior is closer to our expectations. For the cases (diamonds) that acheive a conjugate state bore we can see that the steady-state geometries tend towards values of R that are very close and slightly smaller than the value that would generate no energy jump across the bore according to the naive analysis earlier. For several of the cases with negative shear, we see that bores established with values of R smaller than that which would generate no loss across the bore generate undular bores. In these cases we see that the value of R for the undular bores tends to be smaller than that of conjugate state bores. As the undular bores transmit some energy away from the bore front (the group velocity of the waves is less than the phase velocity of the leading wave of the bore) we would expect this sort of behavior. Returning to the conjugate state cases, if we look at the case when $\Delta\dot{U} = 0.4$ an extra simulation was run with

initial downstream conditions further away from the steady-state geometry. Even in this instance, we see that the bore develops towards similar steady-state geometries; in fact, the final bore geometry is nearly identical for both cases that start with values for R greater than the steady-state value.

Finally switching our attention to the case with a downstream lower layer height greater than half the total channel height (figure 5.8), we see some interesting behavior. Initially, we can see that the bore is undular; as mentioned before, this violates our assumption that the downstream layer height is constant. However, despite this deviation we can still see that the downstream lower layer height reaches a steady state at a value higher than half the total channel height (which is what is seen in all cases without shear). The final bore height is visibly very close to the upper dotted line corresponding to the energy-preserving value for R, supporting our earlier analysis. Although the ratio $R = 1.3$ is not large, there theoretically are energy-preserving cases with a smaller value for r that are also energetically stable. In these cases though the large shear at the downstream interface generates Kelvin-Helmholtz instabilities. Importantly, increasing the shear leads to downstream lower layer heights that are predicted to be greater than half the channel height and decreasing the shear leads to ones less than half the channel height, which is what is seen.

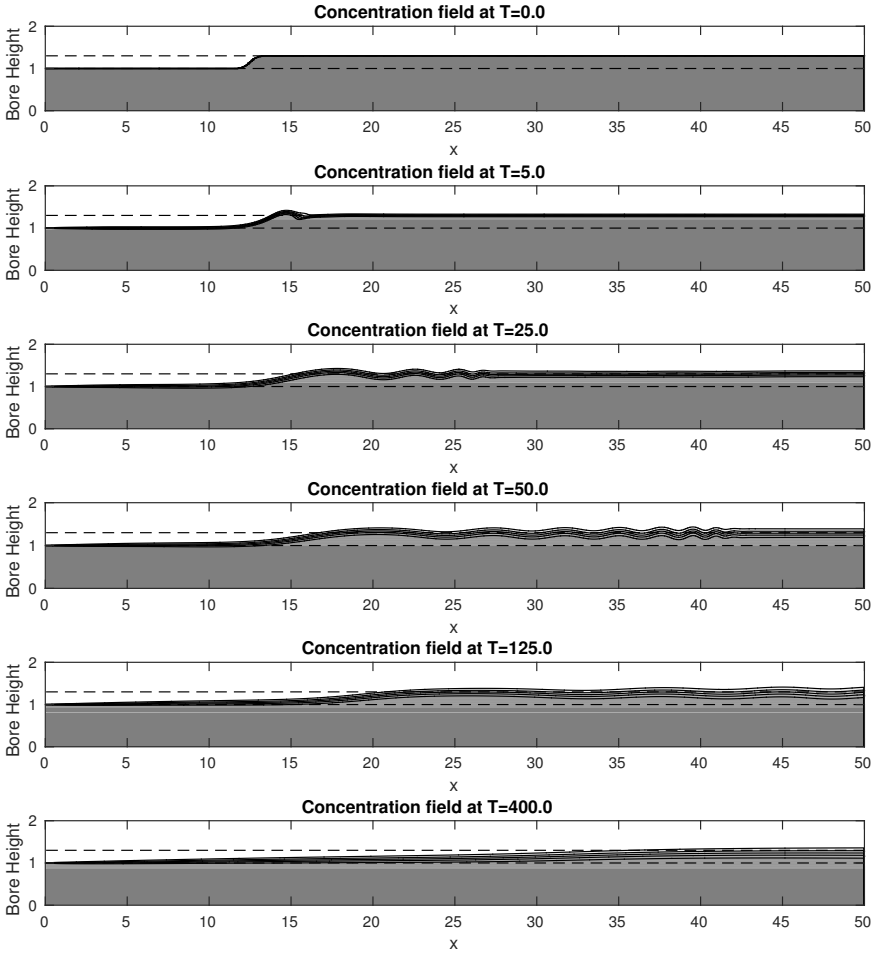

Figure 5.8: Time development of a bore's concentration field with initial parameters $r = 0.5$, $R = 1.3$, and CS $\Delta\dot{U} = 1.0$. This set of parameters is predicted to have no energy change across the bore. The contour lines are set at $\frac{1}{6}$, $\frac{2}{6}$, $\frac{3}{6}$, $\frac{4}{6}$, and $\frac{5}{6}$. The bore moves downstream over time; the difference between the predicted bore velocity of 0.7535 is 0.0452.

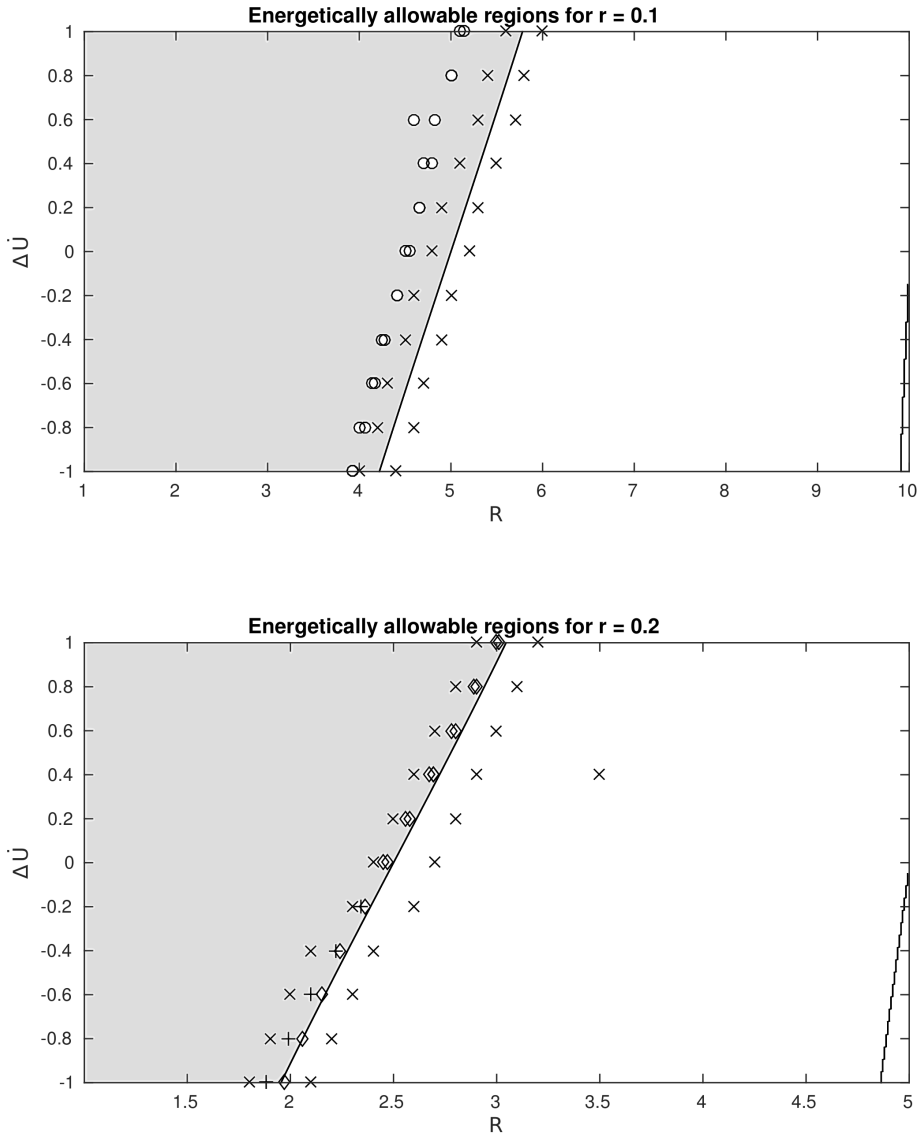

Figure 5.9: Simulations start/ending downstream layer height ratio R along with the CS upstream layer shear $\Delta\dot{U}$. The initial heights are labelled with an x; the steady state heights are labelled with circles, diamonds, and +. Cases with circles develop downstream Kelvin-Helmholtz instabilities; cases with + develop undular waves propagating at a slower velocity than the leading wave; cases with diamonds develop into conjugate state bores. For all cases bores with a larger initial R and the same $\Delta\dot{U}$ have a larger (or equal) final R (then the case with the same initial $\Delta\dot{U}$). For the case when $r = 0.2$, $\Delta\dot{U} = 0.4$, and an initial $R = 3.5$, the final $R = 2.69$. This is identical to the case when $r = 0.2$, $\Delta\dot{U} = 0.4$, and an initial $R = 2.9$. The shaded region is the region with a predicted energy drop across the jump; the central line is the predicted zero-energy line.

Earlier, we conjectured that predicting the steady-state downstream bore parameters from the upsteam parameters would allow us to improve predictions for bore velocity, and thus up to this point we have primarily focused on the steady-state geometry of the bore. We will now proceed to check the accuracy of predicted bore velocities that only use the upstream conditions r and $\Delta\dot{U}$ by using the energy-predicted value for the downstream lower layer height ratio R. Focusing on cases that remain conjugate state, we can compare our velocities predicted using only upstream parameters to the velocities seen in simulations. The results of this comparison is presented in table 5.3. It's important to note that the predicted velocities in the table were done so without any information from the downstream lower layer height ratio R; the predicted R is the value that would generate a bore without any energy loss from our analysis earlier. For this reason the predicted R values are the same for cases with the same upstream parameters; likewise the velocities are also the same for these cases with the same upstream parameters. Focusing on the predicted velocities versus the simulation velocities, we see that the predicted velocities are very close to the simulation velocities. Earlier we saw similar deviations in velocities from when we used the simulation value for R; it appears that using the predicted values for R in the vorticity model can generate accurate predictions for bore velocity using only the upstream parameters.

$\Delta\dot{U}$	Initial R	Energy Predicted R	Final R	R Difference	Simulation Velocity	Energy Predicted Velocity	Energy Predicted Velocity Difference
1.0	2.9	3.0455	3.00	0.04	0.9751	0.9957	0.0206
1.0	3.2	3.0455	3.01	0.03	0.9722	0.9957	0.0235
0.8	2.8	2.9402	2.89	0.05	0.9958	1.0158	0.02
0.8	3.1	2.9402	2.90	0.04	0.9926	1.0158	0.0232
0.6	2.7	2.8324	2.78	0.05	1.0185	1.0381	0.0196
0.6	3	2.8324	2.80	0.03	1.0147	1.0381	0.0234
0.4	2.6	2.7227	2.67	0.05	1.0428	1.0625	0.0197
0.4	2.9	2.7227	2.69	0.03	1.0387	1.0625	0.0238
0.4	3.5	2.7227	2.69	0.03	1.0259	1.0625	0.0366
0.2	2.5	2.6117	2.56	0.05	1.0694	1.0892	0.0198
0.2	2.8	2.6117	2.58	0.03	1.0649	1.0892	0.0243
0.0	2.4	2.5000	2.45	0.05	1.0978	1.118	0.0202
0.0	2.7	2.5000	2.47	0.03	1.0928	1.118	0.0252
-0.2	2.3	2.3883	2.34	0.05	1.1281	1.1492	0.0211
-0.2	2.6	2.3883	2.36	0.03	1.1229	1.1492	0.0263
-0.4*	2.1	2.2773	2.22	0.06	1.1605	1.1825	0.022
-0.4	2.4	2.2773	2.24	0.04	1.1585	1.1825	0.024
-0.6*	2	2.1676	2.10	0.07	1.1946	1.218	0.0234
-0.6	2.3	2.1676	2.15	0.02	1.1926	1.218	0.0254
-0.8*	1.9	2.0598	1.99	0.07	1.2302	1.2558	0.0256
-0.8	2.2	2.0598	2.06	-0.00	1.2284	1.2558	0.0274
-1.0*	1.8	1.9544	1.88	0.07	1.2683	1.2956	0.0273
-1.0	2.1	1.9544	1.97	-0.02	1.2654	1.2956	0.0302

Table 5.1: This table represents the simulation results for various $\Delta\dot{U}$ with $r = 0.2$. Cases with a * on the shear represent that the simulation generated an undular bore. As before, $\Delta\dot{U}$ is the upstream shear, the initial R is the downstream layer ratio that the simulation is initiated with, the final R is the steady-state value for that ratio. In this instance the energy predicted R is the value of R that would generate zero energy loss in our naive analysis based on the upstream parameters. R difference is the difference between these two values of R. The simulation velocity is the nondimensional velocity we found from the simulation, whereas the energy predicted velocity is the nondimensional velocity predicted by the vorticity model using the energy-predicted R. Finally the energy predicted velocity difference is the difference between these two velocities.

Ultimately, the general behavior of CS bores is very similar to the behavior of SJ bores. For cases with initial downstream layer heights either slightly smaller than energy-preserving layer heights or with a predicted energy increase across the bore, we see that the bore remains conjugate state and adapts towards the energy-preserving parameters. Comparing a case with more shear to one with less shear, we again see that the steady lower layer height downstream of the bore is larger for the case with greater shear. Lastly, by putting the parameters of the predicted energy-preserving case into the velocities predicted by the circulation model in section 2.1 we can get excellent agreement between model predictions and simulation behavior without any reference to information downstream of the bore.

5.4 Influence of Reynolds number

The vorticity model assumes inviscid flow conditions and vanishing diffusion. Alternatively, the DNS simulations employ finite Reynolds and Schmidt numbers; this leads to diffuse interfaces and viscous dissipation. Consequently, we would expect some differences between the model predictions and DNS results. For cases with nonzero viscosity, the zero-energy line in the energy analysis will overestimate the actual energy downstream of the bore; within the simulation, there would be a net energy drop across the bore. To investi-

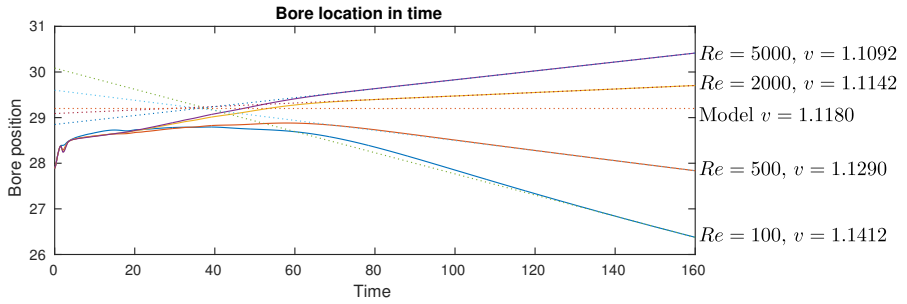

Figure 5.10: Bore front location with $r = 0.2$, $R = 3$, and a shear jump of $\Delta\dot{U} = 0.447$. The bore front is determined by where the depth-integrated height of the lower layer is the average of h_a and h_f. At Re=5000, Kelvin-Helmholtz instabilities develop and slow the bore; at Re=2000, the bore is slightly slower than predicted; at Re=500, the bore height after the jump shrinks, with the new velocity matching the model's predicted velocity for the new parameters; at Re=100, the bore shrinks further (and has a corresponding increase in velocity).

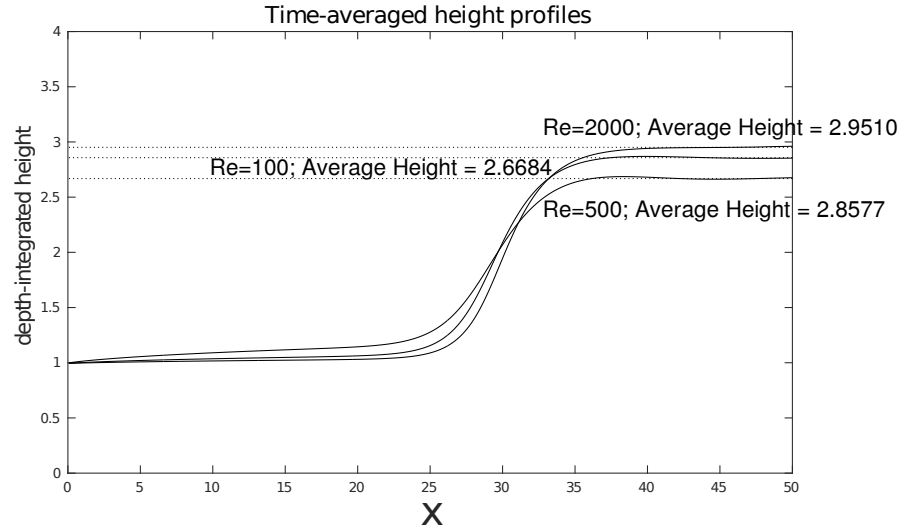

Figure 5.11: Time- and depth- averaged bore height with $r = 0.2$, $R = 3$, and a shear jump of $\Delta\dot{U} = 0.447$. The bore height is determined by taking an average of the time-averaged height from $t = 60$ to $t = 80$ downstream of the bore.

gate this effect, we ran multiple simulations for the same set of parameters for a range of Reynolds numbers (Re=100, 500, 2000, 5000), the results of which can be seen in figure 5.10. For the given initial geometry, the vorticity model predicted that there would be no change in energy across the bore (again ignoring possible energy sinks or other ways to take energy out of the system), thus the geometry would not change. We would expect the simulation results to match our model the closest in the cases with less viscosity (higher Re) so long as the bore remains conjugate state. Because the simulation reference frame is moving with the predicted bore velocity, the positions in figure 5.10 are the differences between predicted and simulated positions unless otherwise stated. However, the velocities given are the velocities from the lab reference frame (the velocities are not relative to the bore velocity).

Looking at figure 5.10, we see that the bore velocity of the Re=2000 case matches the model velocity very closely; the velocity differs by less than $\frac{1}{2}\%$. If we look at figure 5.11, we can furthermore see that the bore height is very close to what is predicted: R develops to be 2.9510 rather than 3. Even this slight deviation makes sense: as mentioned earlier, the predicted zero energy line completely neglects viscosity, so in a simulation we would expect our estimates to consistently be slightly larger than what is seen.

However, for the higher Re case (Re=5000) we see that the bore slows. For this case, Kelvin-Helmholtz instabilities are generated which effect both the energy analysis and violate the assumptions that were made to predict the bore velocity; we will look further at such cases later in section 6.1.

What we see for the cases with greater viscous energy dissipation is that the bore shrinks when compared to cases with less viscous dissipation. The original set of parameters would need a net external energy input to be stable (to overcome this dissipation) so the resulting flow adapts to a different energetically stable condition. This corresponds to an energy drop across the entire domain of figures 5.4 and 5.7, which shifts the energy-preserving contour to the left (corresponding to a smaller R.). Looking at figure 5.11, the bore shrinks in both the Re=500 and the Re=100 case, though the bore shrinks further for the Re=100 case (corresponding to a greater needed external energy input) as can be seen in figure 5.11. For this particular set of parameters ($r = 0.2, R = 2.5, \Delta\dot{U} = 0.447$) a drop in R corresponds to a faster bore velocity (and a larger drop corresponds to a greater increase in velocity). Returning to our simulation results, we see that the conjugate-state cases with a lower Re (which shrink) move faster than cases with a higher Re. Furthermore, the bore sees a subsequent increase in velocity as it shrinks further. However, even in the simulation with the most viscous dissipation ($Re = 100$), the bore

velocity predicted by our model was less than 2% away from our predicted velocity. If we look at figure 2.4 we can see that moving small amounts to the left of the zero energy loss line (a small decrease in R) results in a small increase in bore velocity. Turning our attention to the simulation results and looking at the $Re = 500$ case, the bore shrinks to $R = 2.8576$; if this number is used in the velocity prediction for the circulation model the bore is predicted to move with a velocity $\dot{U} = 1.1394$. This is faster than the $\dot{U} = 1.1290$ seen in the simulation. Likewise, the predicted velocity for the bore as it develops in the $Re = 100$ case is $\dot{U} = 1.1579$ as compared to the $\dot{U} = 1.1412$ we see in our simulations. These two simulations move with a velocity within 1% of predictions if the changing R is accounted for.

5.5 Conjugate state conclusions

Focusing on bores that are close to the zero-energy line (and thus behave as conjugate state bores and match our earlier assumptions) we would expect that within any simulations that energy coming into the control volume is balanced by energy coming out of the control volume, ignoring the small amount of viscous dissipation. A steady bore needs to achieve an energy balance: energy into the control volume needs to either dissipate or exit the control volume. Continuing to ignore the viscous dissipation of energy, a bore will

achieve an energy balance by changing to a new set of geometric parameters. Of the parameters governing the bore, the shear upstream of the bore (magnitude and type) as well as the height of the fluid layers upstream of the bore are fixed by the inflow condition; the only free variable governing the flow is R, which relates to the downstream layer heights. Thus, in conjugate state bores with initial conditions that are not energy preserving, we would expect the bore to grow or shrink towards an energy-conserving set of parameters. The bore should shift left or right in the parameter space seen in figures 5.4 and 5.7 to the point where the energy change is zero. This will generate two interesting predictions for conjugate state bores. The first is that a given set of inflow parameters ($\Delta\dot{U}$ and r) will generate bores that converge to the same height, regardless of the initial starting height after the bore (assuming that the heights are suitably close to the zero energy line that the bore remains a conjugate state bore). The second is that a case with more positive/negative shear upstream of the bore will be larger/smaller than an equivalent case without shear (as the zero energy line shifts towards larger R for larger $\Delta\dot{U}$). In other words, a bore propagating into positive (negative) shear, either a shear jump or a continuous shear gradient, will have a larger lower layer height downstream of the bore than one propagating without shear. This second prediction has been seen in earlier work (Stastna and Lamb, 2002). Furthermore, although

we ignored viscous losses in our energy analysis, the circulation model coupled with the energy analysis gave accurate predictions for the bore velocity even in simulations with significant viscous losses. Ultimately, our work can accurately predict conjugate state bore velocities because our analysis predicts the steady state downstream layer heights.

Until this point in the paper we have been neglecting other methods of energy dissipation; returning to cases that have some viscous dissipation, the net result would be to shift the zero energy line from our naive analysis to the left (smaller values of R). Although this will result in the bore adjusting itself to layer heights that conserves energy which are smaller than predicted (the lower layer height downstream of the bore will shrink as compared to cases without significant viscous dissipation), the general behavior will be the same: conjugate state bores will have a set of geometric parameters that conserve energy, and conjugate state bores that initially do not conserve energy will have the layer heights upstream of the bore change until this energy-preserving set of parameters is reached. Even in this instance though the naive implementation of the energy analysis in Section 4 in coordination with the velocities predicted by the circulation model for the energy-preserving set of parameters can accurately predict the bore velocity.

Chapter 6

Non conjugate state behavior

Earlier, we focused on conjugate state behavior because it matches the assumptions we made in our analysis. In the following sections, we will analyze cases where these assumptions are violated either because there is significant turbulent mixing or because there are multiple wavefronts following the bore. This latter is called an undular bore.

6.1 Turbulent behavior

Earlier, we showed that the initial conditions do not have a large effect on the steady-state behavior of a conjugate state bore: different initial conditions converge to the same behavior. However, the same is not true of turbulent bores, which makes it more difficult to compare simulation results to theory.

Moreover, in turbulent bores many of our assumptions are violated - there is significant viscous mixing, and the downstream layer heights are decidedly not smooth.

In previous simulations, we purposefully kept the Reynolds number low to try to prevent Kelvin-Helmholtz instabilities from forming. In section 5.4, we investigated the effect lowering the Reynolds number had on a bore. Within that section, we briefly mentioned that Kelvin-Helmholtz instabilities developed at the highest Reynolds number we looked at (Re=5000). If we look at figures 5.10 and 5.11, we see that increasing the Reynolds number to the point where Kelvin-Helmholtz instabilities form has an effect on the behavior of the bore by slowing the bore down. Furthermore, increasing the Reynolds number further generates larger instabilities, which will further alter the bore's behavior. In this instance, we can see that for cases with relatively "small" instabilities the circulation model makes a good prediction for the bore velocity despite violations of some of our initial assumptions. Interestingly, even for cases with large instabilities we still see that the velocity predictions made by the circulation model are not poor.

However, applying our earlier methods to predict bore geometry and behavior are not appropriate to bores exhibiting turbulent behavior; different

initial conditions lead to different bore behavior and geometry. This means that wider generalizations are difficult.

6.2 Undular bores

Earlier, we touched upon the necessity of starting simulations close to the zero energy line (with smaller R) to see conjugate state behavior. For cases with high shear, this was necessary because Kelvin-Helmholtz instabilities are generated downstream of the bore, which in turn effect the bore's behavior. This is further investigated in section 6.1. However, for cases with relatively low downstream shear alternate bore behavior occurs that violates our assumptions of constant layer heights. If we look at figure 5.8, we can see that there appears to be a propagation of waves downstream of the bore. This is an example of an undular bore, which occured in both the SJ and CS cases. As the bore develops in time, we see that the longer wavelengths remain closer to the bore front, while shorter wavelengths are transported downstream. This ultimately leads to a group velocity of the wave packet that is less than the velocity of the leading edge of the wave (the bore) which results in a net transport of energy away from the bore.

Included in several earlier tables were the results of cases that generated undular bores. We see that while cases with undular bores see a difference

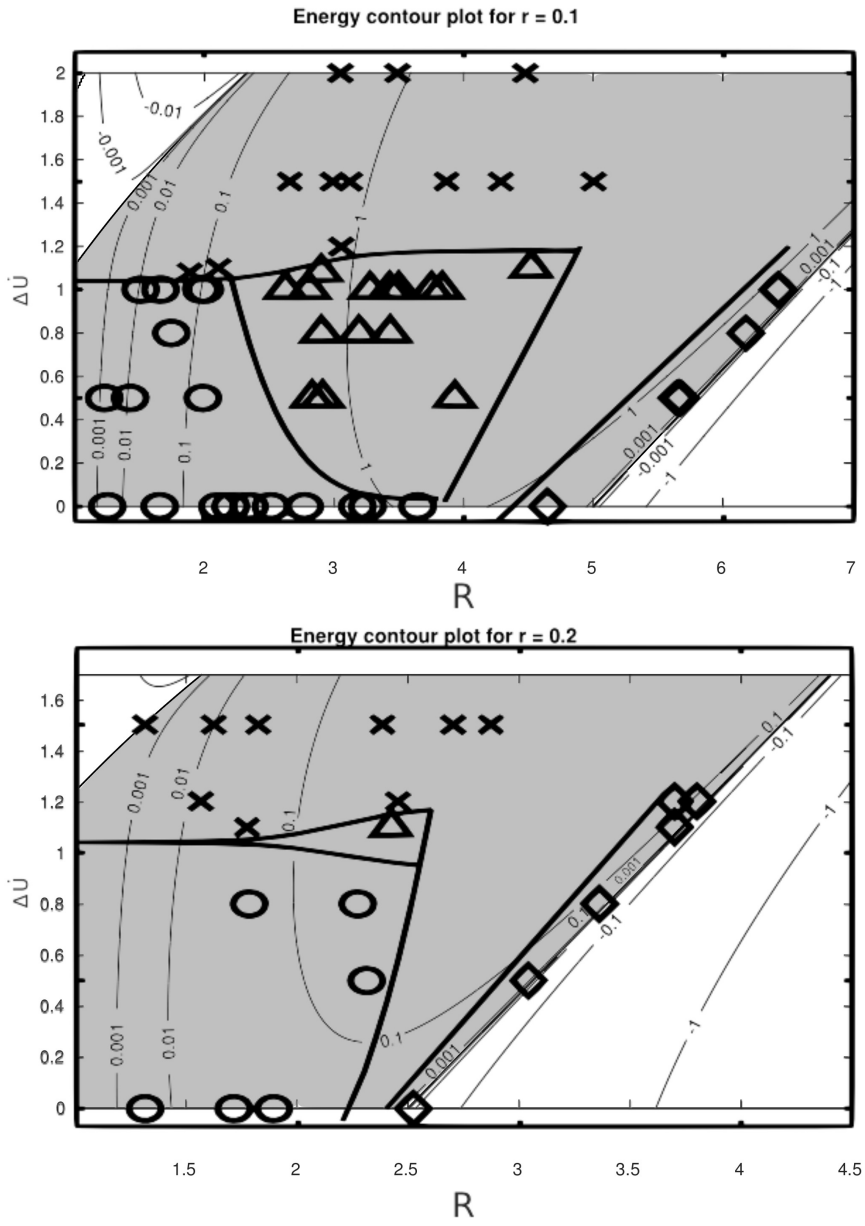

Figure 6.1: Energy contour plots for the shear jump case. $r = 0.1$, $r = 0.2$ from top to bottom. $\Delta\dot{U}$ is on the y axis, R is on the x axis. The light grey shaded region has a predicted energy drop across the bore. Each point represents the result of a numerical simulation from Ogden and Helfrich (2016). $\times$ = fully turbulent jump, $\circ$ = undular bore, $\triangle$= smooth front turbulent jump, and $\diamond$ = conjugate state.

in R compared to their conjugate state counterparts with the same upstream parameters, the bore velocities predicted using the simulation downstream layer height ratio R predicts the velocities for undular bores roughly as well as the velocity of conjugate state bores. Using the energetically predicted value for R decreases slightly the accuracy of the prediction, but the energy predicted velocity is still roughly correct. This is interesting; it suggests that if there were a way to predict R for undular bores in the same way as for conjugate state bores, we could predict their ultimate velocity. The difficulty arises in the development of these undular bores: we see that the same initial conditions can lead to two different outcomes (undular or conjugate state) depending on whether the downstream layer height ratio is above or below the energy-preserving value. More confusingly, undular bores develop to look like conjugate state bores as the shorter wavelengths are convected downstream, and if these waves are convected out of our domain it is not certain that our simulations are valid. Finally, multiple steady undular bores can develop that have the same upstream parameters: in figure 6.1 we can see the results from Ogden and Helfrich (2016), which show multiple steady undular bores at constant r and $\Delta\dot{U}$. Each of these cases can achieve steady behavior without violating any of our assumptions because different amounts of energy can be transported by the waves downstream, but it makes it difficult to apply

our model for conjugate state bores to bores that start with a parameter R significantly smaller than the conjugate state steady value.

Bibliography

Borden, Z. and Meiburg, E. (2013). Circulation-based models for Boussinesq internal bores. *Journal of Fluid Mechanics*, 726:R1.

Hartel, C., Meiburg, E., and Necker, F. (2000). Analysis and direct numerical simulation of the flow at a gravity-current head. part 1. flow topology and front speed for slip and no-slip boundaries. *Journal of Fluid Mechanics*, 418:189–212.

Huerre, P. and Monkewitz, P. A. (1990). Local and global instabilities in spatially developing flows. *Annual Review of Fluid Mechanics*, 22(1):473–537.

Klemp, J. B., Rotunno, R., and Skamarock, W. C. (1997). On the propagation of internal bores. *Journal of Fluid Mechanics*, 331:81–106.

Li, M. and Cummins, P. F. (1998). A note on hydraulic theory of internal bores. *Dynamics of Atmospheres and Oceans*, 28(1):1–7.

Nasr-Azadani, M. M., Hall, B., and Meiburg, E. (2013). Polydisperse turbidity currents propagating over complex topography: comparison of experimental and depth-resolved simulation results. *Computers & Geosciences*, 53:141–153.

Nasr-Azadani, M. M. and Meiburg, E. (2011). TURBINS: an immersed boundary, Navier–Stokes code for the simulation of gravity and turbidity currents interacting with complex topographies. *Computers & Fluids*, 45(1):14–28.

Nasr-Azadani, M. M. and Meiburg, E. (2015). Gravity currents propagating into shear. *Journal of Fluid Mechanics*, 778:552–585.

Ogden, K. A. and Helfrich, K. R. (2016). Internal hydraulic jumps in two-layer flows with upstream shear. *Journal of Fluid Mechanics*, 789:64–92.

Rayleigh, L. (1914). On the theory of long waves and bores. *Proceedings of the Royal Society of London. Series A, Containing Papers of a Mathematical and Physical Character*, 90(619):324–328.

Stastna, M. and Lamb, K. G. (2002). Vortex shedding and sediment resuspension associated with the interaction of an internal solitary wave and the bottom boundary layer. *Geophysical Research Letters*, 29(11).

Wood, I. and Simpson, J. (1984). Jumps in layered miscible fluids. *Journal of Fluid Mechanics*, 140:329–342.